

# Quantum many-body scars in spin models with multibody interactions

Kazuyuki Sanada <sup>1</sup>, Yuan Miao <sup>2</sup>, and Hosho Katsura <sup>1,3,4</sup>

<sup>1</sup>*Department of Physics, Graduate School of Science, The University of Tokyo, 7-3-1 Hongo, Bunkyo-ku, Tokyo 113-0033, Japan*

<sup>2</sup>*Galileo Galilei Institute for Theoretical Physics, INFN, Largo Enrico Fermi 2, 50125 Firenze, Italy*

<sup>3</sup>*Institute for Physics of Intelligence, The University of Tokyo, 7-3-1 Hongo, Bunkyo-ku, Tokyo 113-0033, Japan*

<sup>4</sup>*Trans-scale Quantum Science Institute, The University of Tokyo, Bunkyo-ku, Tokyo 113-0033, Japan*



(Received 13 May 2023; revised 11 September 2023; accepted 12 September 2023; published 2 October 2023)

We introduce and study several classes of quantum spin models with multibody interactions that exhibit quantum many-body scars. The models are constructed by two different methods: one exploiting boundary states in integrable spin chains and the other based on a variant of existing methods such as restricted spectrum generating algebras. The first method allows us to construct deformations of the Majumdar-Ghosh and Affleck-Kennedy-Lieb-Tasaki models—prototypes of frustration-free systems. With the second method, we construct a large class of spin-1 models involving scalar spin chirality in both one and two dimensions. Interestingly, in some cases, the models so constructed have towers of scar states of different character. For each example, we show that the scar states behave differently from thermal states by comparing their spectral and dynamical properties with those of other states. We also show that a superposition of the scar states constructed by the second method exhibits perfectly periodic revivals in the dynamics.

DOI: [10.1103/PhysRevB.108.155102](https://doi.org/10.1103/PhysRevB.108.155102)

## I. INTRODUCTION

Since the early days of quantum mechanics, thermalization of isolated quantum systems has been of great theoretical interest, as it is at the heart of statistical mechanics. Recently, thanks to the development of quantum simulators such as systems with ultracold atoms [1], superconducting circuits [2], trapped ions [3], and Rydberg atoms [4], we have been able to delve into the quantum many-body dynamics in detail, leading to a better understanding of the nature of thermalization. Theoretically, the eigenstate thermalization hypothesis (ETH) was introduced as a plausible mechanism to explain thermalization phenomena in isolated quantum systems [5–7], and was subsequently discussed in a number of papers such as Refs. [8–12]. Roughly speaking, the ETH is a quantum counterpart of ergodicity in classical systems [13,14]. The strong version of ETH asserts that all energy eigenstates are thermal states [15], which are locally indistinguishable from the microcanonical average. It has been confirmed by numerical calculations that the ETH is valid for many isolated quantum systems [16–18].

Even though the ETH has been tested and confirmed in many studies, it does not hold in some special cases [19]. For example, quantum integrable models and many-body localized systems are known to violate the strong ETH [18]. Moreover, there are systems that do not have these characteristics but still have eigenstates that do not thermalize. These nonthermal states are called quantum many-body scars (QMBS) [20–22].

The signatures of QMBS have been observed in recent experiments [4,23,24] and several experimental platforms to realize QMBS have been proposed [25–28]. Of particular interest are systems involving Rydberg atoms [4]. Such systems exhibit nonthermal dynamics, despite being nonintegrable

[29,30]. The theoretical understanding of QMBS has progressed rapidly in recent years, and to date, many models with exact QMBS have been known. Examples include the PXP model [31–33], the Affleck-Kennedy-Lieb-Tasaki (AKLT) model [34–36], the Ising- and XY-like models [37–39], the perturbed Potts model [40], and the Onsager scars [41] (see Ref. [21] for a review). They motivated the development of systematic methods for constructing concrete models with exact QMBS [42–50]. Also, the fate of exact QMBS under perturbations has been a subject of debate [51–53]. For a more mathematical approach, an attempt has been made to comprehensively understand QMBS using commutant algebras [54,55]. However, despite these developments, the overall picture is far from complete. Therefore, to better understand the general framework and origin of QMBS, it is important to explore different methods for constructing new models that host QMBS in a systematic manner.

In this paper, we introduce and study several classes of spin models with multibody interactions that exhibit QMBS. To construct the models, we employ two different methods: one based on integrable boundary states [56–61], and the other using a variant of the existing methods based on restricted spectrum generating algebras [62,63] or quasismmetry groups [46]. The first method allows one to construct an infinite family of models with a scar state. However, since this approach heavily relies on the integrability of some terms in the Hamiltonian, its application is limited to one dimension. In addition, with this method, one cannot obtain a tower of scar states with equal energy spacing. In contrast, the second method allows for the construction of models with towers of scar states. We will demonstrate that a superposition of these scar states shows perfectly periodic revivals in the dynamics. Unlike the first method, the second method is capable of constructing models in higher dimensions. We will illustrate this

using a model on a triangular lattice as an example. It should be noted that both methods allow the models to accommodate designed inhomogeneities that do not affect QMBS.

The paper is organized as follows. In Sec. II A, we explain the two methods in more detail. In Sec. II B, we discuss how to distinguish QMBS from thermal states. In Sec. III, we consider the spin-1/2 Majumdar-Ghosh model deformed by the spin-1/2 scalar spin chirality as an example of a scarred model constructed by the first method. In Sec. IV, we show another example constructed by the same method, namely, the spin-1 AKLT model deformed by the third conserved quantity of the SU(3) Sutherland model. We also discuss possible generalizations to higher spins. In Sec. V, we introduce a model consisting of the AKLT Hamiltonian and the spin-1 scalar spin chirality as an example of a model constructed by the second method. In Sec. VI, we first construct exact zero-energy eigenstates of the spin-1 scalar spin chirality term. Then we show that they form towers of scar states in a class of models obtained by perturbing the scalar spin chirality by tailored disorder and discuss that they are examples of models constructed by the second method. We conclude with a summary and some open questions in Sec. VII. Some technical details are relegated to the Appendices.

## II. METHODS

### A. Construction of scarred models

To construct models with QMBS, we adopt the following two methods (i) the method based on integrable boundary states [57–61], and (ii) the method relying on a tower of states generated by some operator. First, let us describe (i), which is deeply related to quantum integrable systems. Let  $H$  be a nearest-neighbor integrable Hamiltonian. One can construct an infinite number of conserved quantities  $Q_n$  successively starting from  $Q_2 \propto H$  by  $Q_{n+1} = [B, Q_n]$ , where  $B$  is the boost operator [64–67]. Each operator  $Q_n$  can be written as a sum of local operators spanning at most  $n$  consecutive sites. The conserved quantities can be divided into two groups by their behavior under spatial reflection. The even ones,  $Q_{2n}$ , are symmetric under the parity operation, whereas the odd ones  $Q_{2n+1}$  are antisymmetric.

An integrable boundary state, say  $|\Psi_0\rangle$ , is defined as a state that is annihilated by all odd conserved charges [57], i.e.,

$$Q_{2k+1}|\Psi_0\rangle = 0 \quad (1)$$

for all  $k = 1, 2, \dots$ . One can see that if  $|\Psi_0\rangle$  is an energy eigenstate of another Hamiltonian  $H_0$ , then  $|\Psi_0\rangle$  is an exact eigenstate of the Hamiltonian

$$H(t_1, t_2, \dots, t_n) = H_0 + \sum_{k=1}^n t_k Q_{2k+1}, \quad (2)$$

where  $\{t_k\}_{k=1}^n$  are real numbers. If this new Hamiltonian is nonintegrable and the energy of  $|\Psi_0\rangle$  is in the middle of the spectrum, then  $|\Psi_0\rangle$  is likely to be a scar state. Note that this method allows one to construct an enormous number of scarred models by changing parameters  $\{t_k\}_{k=1}^n$ .

Next, we describe the second approach (ii). This is a variant of the existing methods [41,46,62,63]. We first assume that the tower of states generated by an operator  $Q$ , namely,  $Q|\psi\rangle, Q^2|\psi\rangle, Q^3|\psi\rangle, \dots, Q^n|\psi\rangle$ , are energy eigenstates of some Hamiltonian  $H$ . Then, we can create the system with QMBS by considering the property of operator  $Q$  other than each eigenstate. To be more specific, if there exists an operator  $\Pi$  such that  $\Pi Q^k|\psi\rangle = \lambda_k Q^k|\psi\rangle$  ( $\lambda_k \in \mathbb{R}$ ) for all  $k = 0, 1, 2, \dots, n$ , each  $Q^k|\psi\rangle$  is also an eigenstate of the new Hamiltonian  $H' = H + \Pi$ . However, almost all eigenstates of  $H$  are no longer eigenstates of  $H'$ . Thus, it is highly likely that  $Q^k|\psi\rangle$  are the only nonthermal eigenstates of the Hamiltonian  $H'$ .

### B. Numerical verification

To discuss whether a given model has QMBS or not, we need to answer at least the following two questions:

- (1) Is the model nonintegrable?
- (2) Are the likely scar states nonthermal?

We can answer the first question by checking the level-spacing distribution. It is defined as follows. Let  $E_1 \leq E_2 \leq \dots \leq E_N$  be the eigenenergies of a Hamiltonian in ascending order. The normalized level spacing  $s_i$  is then defined as  $s_i := (E_{i+1} - E_i)/\delta$ , where  $\delta := (E_N - E_1)/(N - 1)$  denotes the average over all neighboring level spacings. Then, the level-spacing distribution function  $P(s)$  is defined such that  $P(s)\Delta s$  is the probability of finding  $s_i$  in the interval  $[s, s + \Delta s]$ . It is empirically known that the level-spacing distribution follows the Poisson distribution

$$P(s)_{\text{Poisson}} = e^{-s} \quad (3)$$

for integrable systems [68], whereas for nonintegrable models, it follows the Gaussian orthogonal ensemble (GOE)

$$P(s)_{\text{GOE}} = \frac{\pi}{2} s e^{-\frac{\pi}{4}s^2} \quad (4)$$

for a Hamiltonian with time-reversal symmetry, or it follows the Gaussian unitary ensemble (GUE)

$$P(s)_{\text{GUE}} = \frac{32}{\pi^2} s^2 e^{-\frac{4}{\pi}s^2} \quad (5)$$

for a Hamiltonian without time-reversal symmetry [69–72]. To check which distribution the level spacing follows, we can use  $r$  value other than the histogram of the level spacings  $s_i$  [73]. It is defined as follows. Let  $r_i = \min(s_i/s_{i+1}, s_{i+1}/s_i)$  be a ratio of neighboring level spacings, and let  $\langle r \rangle$  be the  $r$  value, the average of  $r_i$ . By calculating the  $r$  value for each of the distributions, we get  $\langle r_{\text{Poisson}} \rangle = 2 \ln 2 - 1 \approx 0.386$  for Poisson,  $\langle r_{\text{GOE}} \rangle = 4 - 2\sqrt{3} \approx 0.536$  for GOE, and  $\langle r_{\text{GUE}} \rangle = \frac{2\sqrt{3}}{\pi} - \frac{1}{2} \approx 0.603$  for GUE [74].

To answer the second question, we examine several physical quantities for all energy eigenstates. In particular, we use the entanglement entropy as a diagnostic tool to identify nonthermal states. It is defined as follows. Let  $|\psi\rangle$  be a state of the system and let  $A$  be a subsystem. Then the reduced density matrix of  $A$  is defined as  $\rho_A = \text{Tr}_B(|\psi\rangle\langle\psi|)/(|\psi\rangle\langle\psi|)$ , where  $B$  is the complement of  $A$ . The entanglement entropy of  $|\psi\rangle$  is

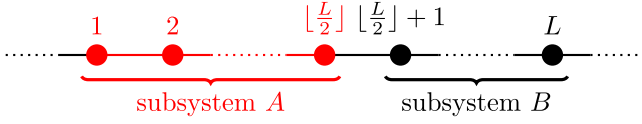


FIG. 1. The definition of subsystems  $A$  and  $B$  for one-dimensional systems. Note that the number of sites in  $A$  is one less than that in  $B$  when  $L$  is odd.

then defined as

$$S_A(|\psi\rangle) = -\text{Tr}_A[\rho_A \ln \rho_A]. \quad (6)$$

It is known that the entanglement entropy of a thermal state obeys a volume law, i.e.,  $S_A$  is proportional to the system size [75]. On the other hand, nonthermal states have sub-volume-law entanglement entropy even if they are in the middle of the energy spectrum. Therefore, nonthermal states such as QMBS can be identified as low-entanglement outliers in the plot of energy versus  $S_A$ . In this paper, we calculate the half-system entanglement entropy for one- and two-dimensional systems (see Figs. 1 and 22 below).

### III. SPIN-1/2 MAJUMDAR-GHOSH MODEL + SCALAR SPIN CHIRALITY

This is one example of a scarred model constructed by method (i) in Sec. II A.

#### A. Hamiltonian

In this section, we consider a one-dimensional spin-1/2 model with two- and three-body interactions. The Hamiltonian of the model depends on a parameter  $t \in \mathbb{R}$  and is given by

$$H(t) = H_{\text{MG}} + tC_{\text{SC}}, \quad (7)$$

where

$$H_{\text{MG}} = \sum_{j=1}^L \left[ (\mathbf{S}_j + \mathbf{S}_{j+1} + \mathbf{S}_{j+2})^2 - \frac{3}{4} \right], \quad (8)$$

$$C_{\text{SC}} = \sum_{j=1}^L \mathbf{S}_j \cdot (\mathbf{S}_{j+1} \times \mathbf{S}_{j+2}), \quad (9)$$

and  $\mathbf{S}_j = (S_j^x, S_j^y, S_j^z)$  is the spin-1/2 operator acting on site  $j$ ,

$$S_j^x = \frac{1}{2} \begin{pmatrix} 0 & 1 \\ 1 & 0 \end{pmatrix}_j, \quad S_j^y = \frac{1}{2} \begin{pmatrix} 0 & -i \\ i & 0 \end{pmatrix}_j, \quad S_j^z = \frac{1}{2} \begin{pmatrix} 1 & 0 \\ 0 & -1 \end{pmatrix}_j. \quad (10)$$

We impose periodic boundary conditions and assume that the number of sites  $L$  is even. The first term  $H_{\text{MG}}$  is the Hamiltonian of the Majumdar-Ghosh model exhibiting exact dimer ground states [76–78], while the second term  $C_{\text{SC}}$  is the scalar spin chirality [79]. Note that  $C_{\text{SC}}$  is the third conserved charge of the spin-1/2 Heisenberg model [80]. Physically, this term appears at third order in perturbation theory starting from the SU(2) Hubbard model at half-filling in an external magnetic field [81]. We also note in passing that a similar three-spin

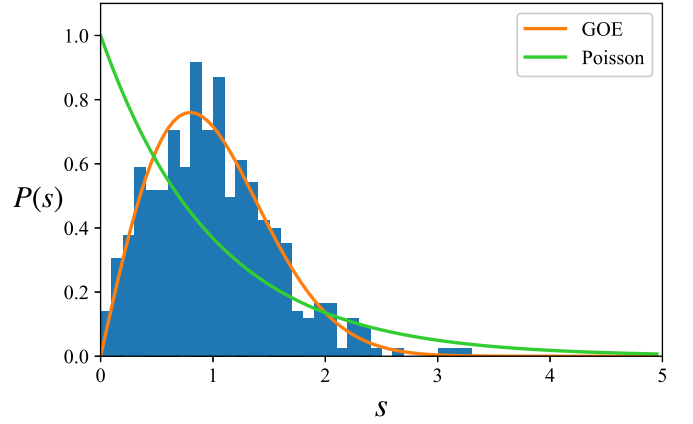


FIG. 2. Level-spacing statistics in the middle half of the spectrum of  $H(t)$  in Eq. (7) with  $t = 8$  and  $L = 20$ . The data are taken in the symmetry sector where  $(S^z, \mathcal{S}, \mathcal{T}, \mathcal{F}) = (0, 0, 1, 1)$ . The curves  $P(s)_{\text{GOE}}$  (orange) and  $P(s)_{\text{Poisson}}$  (green) are shown for comparison. The distribution follows  $P(s)_{\text{GOE}}$ .

interaction has recently been realized experimentally in Rydberg atom arrays [82].

#### B. Symmetries and nonintegrability

The Majumdar-Ghosh model has several symmetries: The Hamiltonian is invariant under time-reversal  $\Theta: \mathbf{S}_j \mapsto -\mathbf{S}_j$ , SU(2) spin rotation, translation  $\mathcal{T}: \mathbf{S}_j \mapsto \mathbf{S}_{j+1}$ , bond-centered inversion  $\mathcal{I}_b: \mathbf{S}_j \mapsto \mathbf{S}_{L-j+1}$ , site-centered inversion  $\mathcal{I}_s: \mathbf{S}_j \mapsto \mathbf{S}_{-j}$ , and spin-flip  $\mathcal{F}: \mathbf{S}_j \mapsto (S_j^x, -S_j^y, -S_j^z)$  [83]. Among these symmetries, time-reversal and bond-centered- and site-centered-inversion symmetries are absent in the scalar spin chirality  $C_{\text{SC}}$ . However, the combination of  $\Theta$  and  $\mathcal{I}_s$  leaves  $C_{\text{SC}}$  invariant, which we call pseudo-time-reversal symmetry. Therefore, the entire model  $H(t)$  has SU(2), translation, spin-flip, and pseudo-time-reversal symmetries. Among them, the first three are unitary symmetries and allow us to diagonalize the Hamiltonian sector by sector. For convenience we define the total spin operators as  $S^\alpha := \sum_{j=1}^L S_j^\alpha$  ( $\alpha = x, y, z$ ) and write the eigenvalue of SU(2) Casimir operator  $\mathbf{S}^2 = \sum_{\alpha=x,y,z} (S^\alpha)^2$  as  $S(S+1)$ . With a slight abuse of notation, we will denote the eigenvalues of the operators  $S^z$ ,  $\mathcal{T}$ , and  $\mathcal{F}$  by the same symbols.

The Hamiltonian Eq. (7) is nonintegrable. This can be shown by studying the level-spacing statistics in a symmetry sector labeled by  $S^z$ ,  $\mathcal{T}$ , and  $\mathcal{F}$ . Figure 2 clearly shows that the level-spacing distribution of  $H(t)$  is close to the GOE Wigner-Dyson distribution. This is consistent with the pseudo-time-reversal symmetry of the model. In addition, the  $r$  value calculated from the histogram in Fig. 2 is  $\langle r \rangle \simeq 0.538$ , which is close to  $\langle r_{\text{GOE}} \rangle$ . Thus, we conclude that the model (7) is nonintegrable.

Figure 3 shows  $\langle r \rangle$  as a function of  $t$  for the model (7) with different system sizes. Clearly, the results for  $L = 18$  and 20 have the same trend. When  $t < 20$ , the  $r$  value  $\langle r \rangle$  is close to the GOE value 0.536, whereas  $\langle r \rangle$  gets closer to the Poisson value 0.386 as  $t$  increases further. This implies that for large  $t$  the whole Hamiltonian (7) is dominated by the integrable part  $tC_{\text{SC}}$  and the system behaves more like an integrable system.

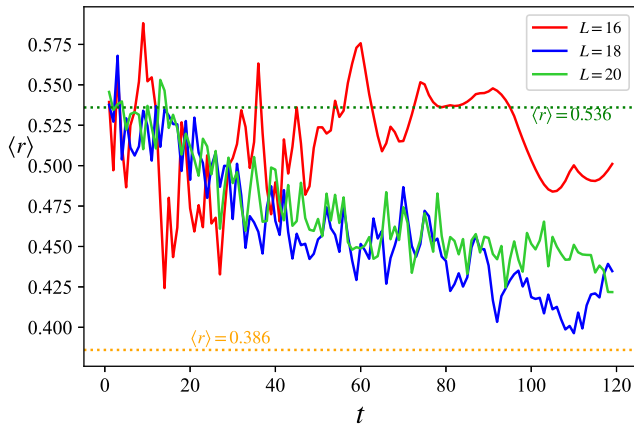


FIG. 3. The mean level-spacing ratio  $\langle r \rangle$  as a function of  $t$  for the Hamiltonian (7) in the symmetry sector  $(\mathcal{S}^z, \mathcal{S}, \mathcal{T}, \mathcal{F}) = (0, 0, 1, 1)$  for  $L = 16, 18,$  and  $20$ . The green and orange dotted lines indicate  $\langle r_{\text{GOE}} \rangle \approx 0.536$  and  $\langle r_{\text{Poisson}} \rangle \approx 0.386$ , respectively.

### C. Scar states

The zero-energy ground states of  $H_{\text{MG}}$  can be written as the following dimer states:

$$|\Psi_1\rangle = |\text{sing}\rangle_{1,2} \otimes |\text{sing}\rangle_{3,4} \otimes \cdots \otimes |\text{sing}\rangle_{L-1,L}, \quad (11)$$

$$|\Psi_2\rangle = |\text{sing}\rangle_{2,3} \otimes |\text{sing}\rangle_{4,5} \otimes \cdots \otimes |\text{sing}\rangle_{L,1}, \quad (12)$$

where  $|\text{sing}\rangle_{i,j} = \frac{1}{\sqrt{2}}(|\uparrow\downarrow\rangle_{i,j} - |\downarrow\uparrow\rangle_{i,j})$  denotes the normalized spin singlet formed between site  $i$  and  $j$ . The two states are related to each other by  $|\Psi_2\rangle = \mathcal{T}|\Psi_1\rangle$ .

As discussed in [57], these states are integrable boundary states of the spin-1/2 Heisenberg XXX chain, meaning that they are annihilated by all parity-odd conserved charges of the Heisenberg Hamiltonian. Since  $C_{\text{SC}}$  is one of the parity-odd conserved charges, it is clear that  $|\Psi_1\rangle$  and  $|\Psi_2\rangle$  are simultaneously annihilated by both  $H_{\text{MG}}$  and  $C_{\text{SC}}$ . Thus they are zero-energy eigenstates of  $H(t)$  in Eq. (7) for all  $t$ . We now argue that the states  $|\Psi_1\rangle$  and  $|\Psi_2\rangle$  can be thought of as QMBS. To this end, we compute the half-chain entanglement entropies ( $S_A$ ) of all energy eigenstates for several system sizes.

Figure 4 shows the results in the subspace spanned by translation-invariant states with zero magnetization, i.e.,

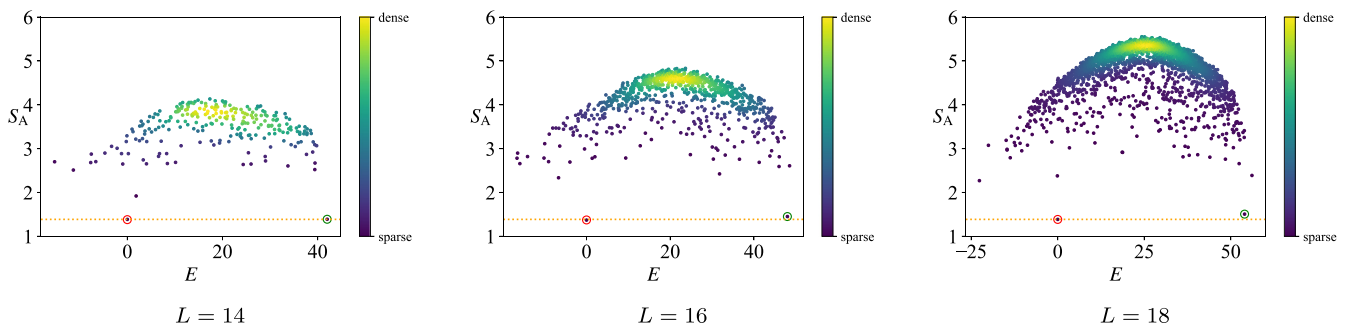


FIG. 4. Entanglement entropy  $S_A$  in all eigenstates of  $H(t)$  in Eq. (7) with  $t = 8$  in the symmetry sector  $(\mathcal{S}^z, \mathcal{T}) = (0, 1)$  for  $L = 14, 16,$  and  $18$ . The density of data points is color coded. The red and green circles indicate the dimer state  $|\text{dimer}\rangle$  and the ferromagnetic state  $|F_{L/2}\rangle$ , respectively. The orange dotted line indicates  $S_A = 2 \ln 2 \simeq 1.386$ .

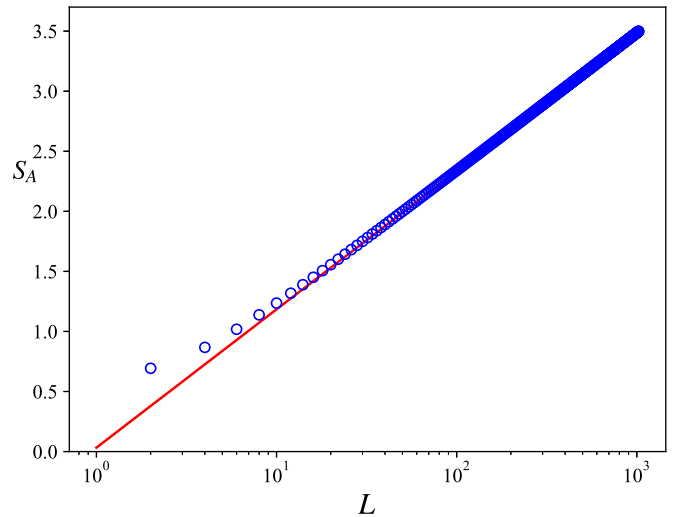


FIG. 5. Size dependence of the half-chain entanglement entropy of the ferromagnetic state  $|F_{L/2}\rangle$ . The red line represents the right-hand side of Eq. (13).

$(\mathcal{S}^z, \mathcal{T}) = (0, 1)$ . Clearly, there is a low-entanglement state distinguished from the other at zero energy. This state can be identified as  $|\text{dimer}\rangle = (2 + (-\frac{1}{2})^{\frac{L}{2}-2})^{-\frac{1}{2}}(|\Psi_1\rangle + |\Psi_2\rangle)$ , which is invariant under translation by one site. It is known that the half-chain entanglement entropy of  $|\text{dimer}\rangle$  becomes  $S_A = 2 \ln 2$  for sufficiently large  $L$  [84]. We can see that the entanglement entropy of the dimer state matches this value. Furthermore, this state remains an outlier from the rest of the states with increasing  $L$ .

We note that the low-entanglement state near the upper edge of the spectrum ( $E = 54$ ) is a ferromagnetic state with zero magnetization written as  $|F_{L/2}\rangle = (\mathcal{S}^-)^{L/2}|\uparrow\rangle$ , where  $\mathcal{S}^- := \mathcal{S}^x - i\mathcal{S}^y$  and  $|\uparrow\rangle$  denotes the all-up state. The asymptotic form of the half-chain entanglement entropy of this state can be read off from Eq. (16) of [85] (see also Appendix A). The result reads

$$S_A(|F_{L/2}\rangle) \approx \frac{1}{2} \ln L + \frac{1}{2} \ln \frac{e\pi}{8} \quad (L \gg 1). \quad (13)$$

Figure 5 shows the size dependence of  $S_A(|F_{L/2}\rangle)$ . It clearly demonstrates that the entanglement entropy obeys a sub-volume law  $S_A \sim \ln(L)$ . For  $L = 18$ , we obtain  $S_A(|F_{L/2}\rangle) \approx$

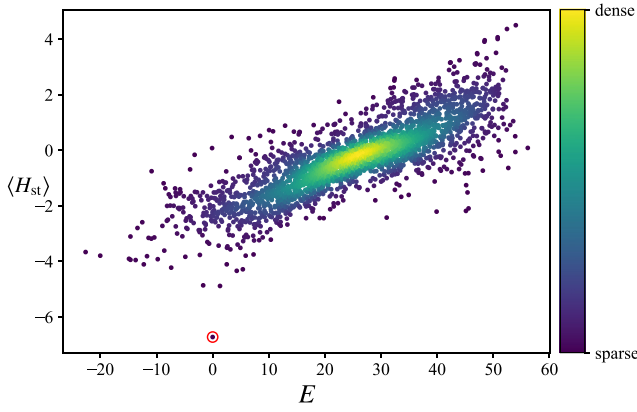


FIG. 6. The expectation values of  $H_{st}$  with  $\epsilon = 0.2$  in all eigenstates of  $H(t)$  in Eq. (7) with  $t = 8$ , and  $L = 18$  in the symmetry sector  $(\mathcal{S}^z, \mathcal{T}) = (0, 1)$ . The density of data points is color coded. The red circle indicates the dimer state  $|\text{dimer}\rangle$  with  $\langle H_{st} \rangle \simeq -6.72$ , which agrees with the analytical value  $\langle H_{st} \rangle = -1143/170$  obtained from Eq. (15).

1.478, which agrees with the numerical result shown by the green circle in Fig. 4. It should be noted that the ferromagnetic state is not an example of a scar state because the state belongs to the subspace with maximum total spin, which is an irreducible representation of the global  $SU(2)$  symmetry of the model Eq. (7).

We remark that since the dimer states are integrable boundary states of the spin-1/2 Heisenberg chain, one can construct other models involving higher-order conserved charges  $Q_{2k+1}$  ( $k > 1$ ), which have the dimer states as QMBS. See Refs. [65,86] for the explicit expressions of  $Q_{2n+1}$ .

Another characteristic of QMBS is that the expectation values of physical quantities in these states do not match the microcanonical averages. Thus, we can identify QMBS by comparing the expectation value of an observable for each energy eigenstate. Here, we choose the staggered Heisenberg Hamiltonian

$$H_{st} = \sum_{j=1}^L (1 + (-1)^j \epsilon) \mathbf{S}_j \cdot \mathbf{S}_{j+1} \quad (14)$$

as a generic observable and calculate the expectation value  $\langle H_{st} \rangle = \langle \psi | H_{st} | \psi \rangle$  for each normalized eigenstate  $|\psi\rangle$  of  $H(t)$  in Eq. (7). Figure 6 shows the numerical results for  $t = 8$  and  $L = 18$  in the symmetry sector  $(\mathcal{S}^z, \mathcal{T}) = (0, 1)$ . They clearly indicate that the expectation value in the dimer state, which is calculated as

$$\langle \text{dimer} | H_{st} | \text{dimer} \rangle = -\frac{3L \left[ \left(-\frac{1}{2}\right)^{\frac{L}{2}} + \frac{1}{4} \right]}{2 + \left(-\frac{1}{2}\right)^{\frac{L}{2}-2}}, \quad (15)$$

is far from those in the states near  $E = 0$ .

Although we have shown the results only for the symmetry sector  $(\mathcal{S}^z, \mathcal{T}) = (0, 1)$ , we note that similar results hold for  $(\mathcal{S}^z, \mathcal{T}) = (0, -1)$ , where  $|\text{dimer}'\rangle \propto |\Psi_1\rangle - |\Psi_2\rangle$  is singled out as a scar state.

#### IV. SPIN-1 AKLT MODEL + $H_3$

This is another example of a model with QMBS constructed by method (i) in Sec. II A.

##### A. Hamiltonian

In this section, we consider a spin-1 model with two- and three-site interactions. Consider a spin-1 chain of length  $L$  with periodic boundary conditions, and let  $\mathbf{S}_j = (S_j^x, S_j^y, S_j^z)$  be the operators of the spin-1 representation of the  $SU(2)$  algebra acting on site  $j$ ,

$$\begin{aligned} S_j^x &= \frac{1}{\sqrt{2}} \begin{pmatrix} 0 & 1 & 0 \\ 1 & 0 & 1 \\ 0 & 1 & 0 \end{pmatrix}_j, \quad S_j^y = \frac{1}{\sqrt{2}} \begin{pmatrix} 0 & -i & 0 \\ i & 0 & -i \\ 0 & i & 0 \end{pmatrix}_j, \\ S_j^z &= \begin{pmatrix} 1 & 0 & 0 \\ 0 & 0 & 0 \\ 0 & 0 & -1 \end{pmatrix}_j. \end{aligned} \quad (16)$$

As usual, we define the total spin operators by  $\mathcal{S}^\alpha := \sum_{j=1}^L S_j^\alpha$  ( $\alpha = x, y, z$ ) and write the eigenvalue of the Casimir operator  $\mathcal{S}^2 = \sum_{\alpha=x,y,z} (\mathcal{S}^\alpha)^2$  as  $\mathcal{S}(\mathcal{S} + 1)$ .

The Hamiltonian of the model is given by

$$H(t) = H_{\text{AKLT}} + tH_3, \quad (17)$$

where

$$H_{\text{AKLT}} = \sum_{j=1}^L \left[ \mathbf{S}_j \cdot \mathbf{S}_{j+1} + \frac{1}{3} (\mathbf{S}_j \cdot \mathbf{S}_{j+1})^2 + \frac{2}{3} \right] \quad (18)$$

is the Affleck-Kenedy-Lieb-Tasaki (AKLT) Hamiltonian [87–89] and

$$H_3 = \sum_{j=1}^L \sum_{a,b,c=1}^8 f_{abc} \lambda_j^a \lambda_{j+1}^b \lambda_{j+2}^c, \quad (19)$$

is the third conserved quantity of the  $SU(3)$  Sutherland model [90–93]. Here  $\lambda_j^a$  ( $a = 1, \dots, 8$ ) represent the Gell-Mann matrices acting on site  $j$ , and  $f_{abc}$  are the structure constants determined by  $[\lambda^a, \lambda^b] = 2if_{abc}\lambda^c$ . The term  $H_3$  is an  $SU(3)$  generalization of the scalar spin chirality. This can be seen by noting that the scalar spin chirality discussed in Sec. III can be rewritten as

$$C_{\text{SC}} = \sum_{j=1}^L \sum_{\substack{a,b,c \\ =x,y,z}} \epsilon_{abc} S_j^a S_{j+1}^b S_{j+2}^c, \quad (20)$$

where  $\epsilon_{abc}$  is the totally antisymmetric tensor, which is also known as the structure constants of the  $SU(2)$  algebra.

There is an interesting alternative expression for  $H_3$ . Let  $P_{i,j}$  be the permutation operator that swaps the state at site  $i$  with the state at site  $j$ ,

$$P_{i,j} |\dots, s_i, \dots, s_j, \dots\rangle = |\dots, s_j, \dots, s_i, \dots\rangle. \quad (21)$$

Here,  $s_i \in \{+, 0, -\}$  denotes the spin state at the site  $i$ . Using  $P_{i,j}$ , we define the three-site ring-exchange operator as

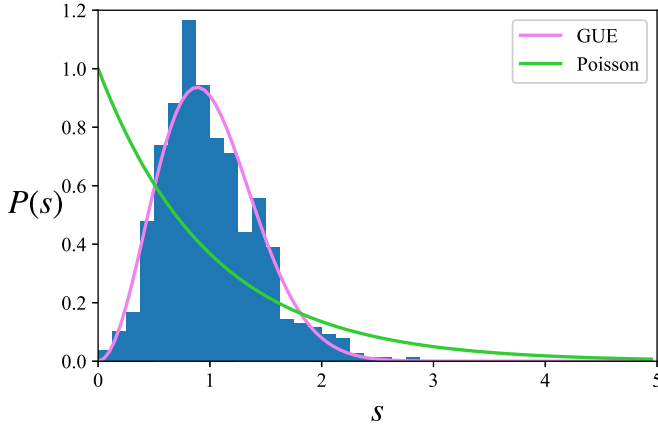


FIG. 7. Level-spacing statistics in the middle half of the spectrum of  $H(t)$  in (17) with  $t = 3$  and  $L = 14$ . The data are taken in the symmetry sector where  $(S^z, \mathcal{S}, \mathcal{T}, \mathcal{F}) = (0, 0, 1, 1)$ . The curves  $P(s)_{\text{GUE}}$  (magenta) and  $P(s)_{\text{Poisson}}$  (green) are shown for comparison. The distribution follows  $P(s)_{\text{GUE}}$ .

$P_{i,j,k} := P_{j,k}P_{i,j}$ . Then the following relation holds [94]:

$$\lambda_i \cdot \lambda_j = 2P_{i,j} - \frac{2}{3}, \quad (22)$$

where  $\lambda_i = (\lambda_i^1, \lambda_i^2, \dots, \lambda_i^8)$  is a collection of the eight Gell-Mann operators acting on site  $i$ . Then, using this relation and  $\sum_c f_{abc} \lambda_{j+2}^c = \frac{1}{2i} [\lambda_{j+2}^a, \lambda_{j+2}^b]$ , we arrive at the alternative expression for  $H_3$  in terms of  $P_{i,j,k}$ ,

$$H_3 = -2i \sum_{j=1}^L (P_{j,j+1,j+2} - P_{j,j+1,j+2}^\dagger), \quad (23)$$

where  $P_{i,j,k}^\dagger = P_{i,j,k}^{-1} = P_{i,j}P_{j,k}$ . We note in passing that there are some studies on spin models containing the SU(3) scalar spin chirality term [95].

### B. Symmetries and nonintegrability

The AKLT Hamiltonian is invariant under time-reversal  $\Theta$ , SU(2) spin rotation, translation  $\mathcal{T}$ , bond-centered inversion  $\mathcal{I}_b$ , site-centered inversion  $\mathcal{I}_s$ , and spin-flip  $\mathcal{F}$ , whereas  $H_3$  lacks time-reversal and inversion symmetries among them [see Appendix B for a discussion of the SU(2) symmetry of  $H_3$ ]. However, the combined symmetry  $\Theta\mathcal{I}_s$  leaves  $H_3$  invariant. Therefore, the model  $H(t)$  in Eq. (17) has SU(2), translation, spin-flip, and pseudo-time-reversal symmetries.

Since the SU(3) Sutherland model is integrable, the third conserved charge  $H_3$  can be considered as a quantum integrable Hamiltonian as well. On the other hand, the AKLT Hamiltonian is nonintegrable. Thus, the model Eq. (17), an interpolation between the two, is expected to be nonintegrable. To verify this, we compute the level-spacing statistics (Fig. 7). The results show that the level-spacing distribution follows the GUE Wigner-Dyson distribution instead of the Poisson distribution, which provides strong evidence that this model is nonintegrable. It can also be checked by the  $r$  value ( $r$ )  $\simeq 0.599$ , which is close to  $\langle r_{\text{GUE}} \rangle \simeq 0.603$ . We remark that the model is expected to belong to the GOE class, as it has pseudo-time-reversal symmetry. The observed discrepancy may be due to the crossover between different

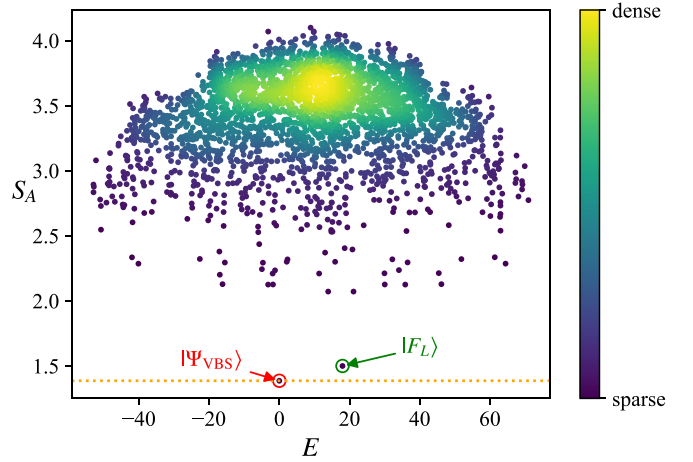


FIG. 8. Entanglement entropies in all eigenstates of  $H(t)$  in Eq. (17) for  $L = 9$ ,  $t = 3$  in the  $S^z = 0$  sector. The density of data points is color coded. The points enclosed by the red and green circles indicate the VBS state  $|\Psi_{\text{VBS}}\rangle$  and ferromagnetic state  $|F_L\rangle$ , respectively. The orange dotted line indicates  $S_A = 2 \ln 2 \simeq 1.386$ .

universality classes [96,97] or finite-size effects, which are also pronounced in the PXP model [29,51].

### C. Scar state

We now argue that the ground state of the AKLT model, known as the valence-bond solid (VBS) state, can be thought of as a scar state. The VBS state can be written as a matrix product state [88].

$$|\Psi_{\text{VBS}}\rangle = \sum_{\{s\}} \text{Tr}[A^{s_1} A^{s_2} \cdots A^{s_L}] |s_1, s_2, \dots, s_L\rangle, \quad (24)$$

where  $s_j \in \{+, 0, -\}$  denotes the spin state at site  $j$  and

$$A^+ = \sqrt{\frac{2}{3}} \sigma^+, A^0 = -\sqrt{\frac{1}{3}} \sigma^z, A^- = -\sqrt{\frac{2}{3}} \sigma^-, \quad (25)$$

with  $\sigma^\pm$  and  $\sigma^z$  being the Pauli matrices. The summation is taken over all possible spin configurations.

The VBS state is an exact ground state of  $H_{\text{AKLT}}$  with zero energy, i.e.,  $H_{\text{AKLT}}|\Psi_{\text{VBS}}\rangle = 0$ . In addition, the VBS state is an integrable boundary state of the Sutherland model (see Appendix C for details). Thus,  $|\Psi_{\text{VBS}}\rangle$  is a zero-energy eigenstate of  $H(t)$  in Eq. (17) for all  $t$  and is likely to be a scar state. In order to establish this, we need to consider the case of moderate  $t$ . This is because, if  $t$  is close to zero, then the energy of the VBS state is near the lower edge of the spectrum. However, such a state cannot be thought of as QMBS, as its energy is not in the bulk of the spectrum. In addition,  $t$  should not be too large so that the model is away from the integrable case ( $H_3$ ). With these in mind, we study the model with  $t = 3$ .

To confirm that the VBS state is indeed a scar state, we numerically compute half-chain entanglement entropies  $S_A$ . The results are shown in Fig. 8. It is known that  $S_A$  of the VBS state is [98,99]

$$S_A(|\Psi_{\text{VBS}}\rangle) = -3\lambda_A \ln \lambda_A - \lambda_B \ln \lambda_B \quad (26)$$

with

$$\lambda_A = \frac{1}{4} \frac{(1 - p^{\lfloor L/2 \rfloor})(1 - p^{\lceil L/2 \rceil})}{1 - p^{L-1}}, \quad (27)$$

$$\lambda_B = \frac{1}{4} \frac{(1 + 3p^{\lfloor L/2 \rfloor})(1 + 3p^{\lceil L/2 \rceil})}{1 - p^{L-1}}, \quad (28)$$

where  $p = -1/3$ .  $\lfloor x \rfloor$  and  $\lceil x \rceil$  denote the floor and ceiling functions, respectively. In the thermodynamic limit, we obtain

$$\lim_{L \rightarrow \infty} S_A(|\Psi_{\text{VBS}}\rangle) = 2 \ln 2. \quad (29)$$

Figure 8 clearly shows that the VBS state at  $E = 0$  with  $S_A \sim 2 \ln 2$  is isolated from the other states, indicating that the VBS state exhibits a different behavior from the other thermal states.

The other low-entanglement state at  $E = 18$  is a ferromagnetic state  $|F_L\rangle$  (see Appendix D). This state is not an example of a scar state because it is a state in the subspace with maximum total spin, which is an irreducible representation of the  $SU(2)$  symmetry of the model Eq. (17).

#### D. Inhomogeneous generalization

In the previous model, it was necessary to increase  $t$  in order to make the energy density of the VBS state (relative to the ground state) finite. However, the problem is that this would increase the effect of  $H_3$  and make the behavior of the system more like that of an integrable system. To avoid such a situation, we consider an inhomogeneous generalization of the AKLT Hamiltonian. In this case, the VBS state is still a zero-energy eigenstate of the inhomogeneous Hamiltonian, yet locating in the middle of the spectrum. The Hamiltonian of the inhomogeneous model is given by

$$\tilde{H}(t) = \tilde{H}_{\text{AKLT}} + tH_3 \quad (30)$$

with

$$\tilde{H}_{\text{AKLT}} = \sum_{j=1}^L c_j \left[ \mathbf{S}_j \cdot \mathbf{S}_{j+1} + \frac{1}{3} (\mathbf{S}_j \cdot \mathbf{S}_{j+1})^2 + \frac{2}{3} \right]. \quad (31)$$

In principle, each coefficient  $c_j$  can be any real number. However, for our purpose, we choose  $|c_j| \lesssim t$  in order to keep the magnitudes of the two terms ( $\tilde{H}_{\text{AKLT}}$  and  $H_3$ ) comparable. In the following, we set  $t \simeq 1$  and draw  $c_j$  uniformly from the interval  $[-1, 1]$ , in which case the model is no longer invariant under the combination of  $\Theta$  and  $\mathcal{I}_s$ .

Like  $H(t)$  in Eq. (17),  $\tilde{H}(t)$  in Eq. (30) is also nonintegrable. As Fig. 9 shows, the level-spacing statistics of the model behave as that of the GUE. Also, the calculated  $r$  value  $r \simeq 0.598$  is compatible with the  $r$  value of the GUE  $\langle r_{\text{GUE}} \rangle \simeq 0.603$ .

#### I. Entanglement entropy

In order to check whether the VBS state is a scar state, we compute entanglement entropies. The results are shown in Fig. 10. Clearly, there are two entanglement outliers. The one at  $E = 0$  is the VBS state. The other one that is also far from other ordinary states is the ferromagnetic state. Its energy is  $2 \sum c_j$  (see Appendix D), and it is a trivial state rather than a scar because of the  $SU(2)$  symmetry of the model (30).

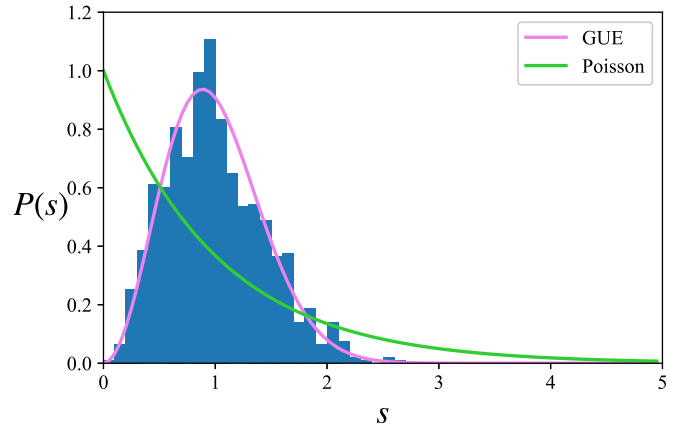


FIG. 9. Level-spacing statistics in the middle half of the spectrum of the inhomogeneous model  $\tilde{H}(t)$  in Eq. (30) with  $t = 1$  and  $L = 11$ . Each  $c_j$  is randomly chosen from  $[-1, 1]$ . The data are taken in the symmetry sector where  $(S^z, \mathcal{S}, \mathcal{F}) = (0, 0, 1)$ . The curves  $P(s)_{\text{GUE}}$  (magenta) and  $P(s)_{\text{Poisson}}$  (green) are shown for comparison. The distribution follows  $P(s)_{\text{GUE}}$ .

#### 2. Other thermodynamic quantities

We provide further evidence that the VBS state is a scar state in this model. To this end, we study the expectation values of some physical observable in all energy eigenstates. The physical quantity we consider here is the AKLT Hamiltonian Eq. (18) whose expectation value in a normalized state  $|\psi\rangle$  is denoted as  $\langle H_{\text{AKLT}} \rangle := \langle \psi | H_{\text{AKLT}} | \psi \rangle$ . Figure 11 shows the numerical result for the distribution of  $\langle H_{\text{AKLT}} \rangle$ . Clearly, the VBS state at  $(0,0)$  can be distinguished from other eigenstates.

#### E. Further generalizations

Now we generalize the model in the previous subsection in two ways. First, we consider a generalization of the spin-1 AKLT model to include next-nearest-neighbor interactions. Based on the results obtained in [100,101], we find that the

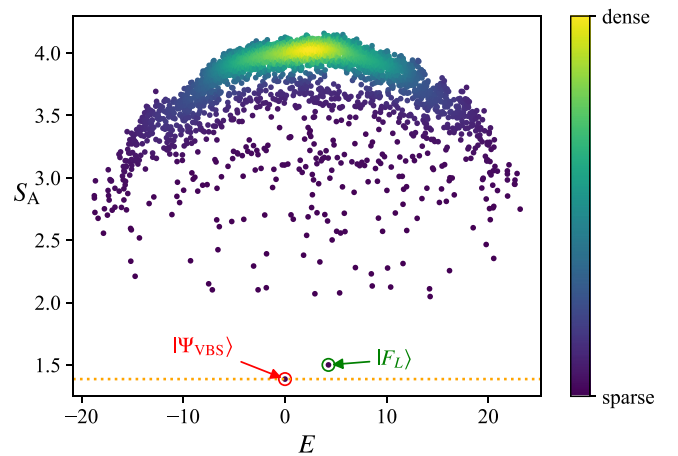


FIG. 10. Entanglement entropies in all eigenstates of the inhomogeneous model  $\tilde{H}(t)$  in Eq. (30) for  $L = 9$ ,  $t = 1$  in the  $S^z = 0$  sector. The density of data points is color coded. Each  $c_j$  is randomly chosen from  $[-1, 1]$ . The red and green circles indicate the VBS and the ferromagnetic states, respectively.

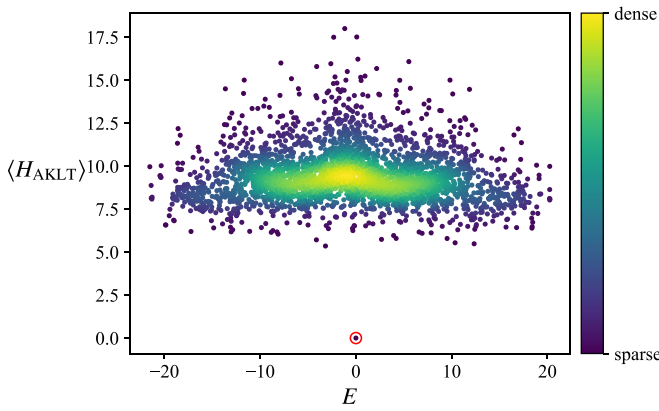


FIG. 11. The expectation values of  $H_{AKLT}$  in all eigenstates of (30) with  $t = 1$ ,  $L = 9$  in the symmetry sector where  $\mathcal{S}^z = 0$ . The density of data points is color coded. The red circle indicates the VBS state.

VBS state in Eq. (24) is annihilated by

$$\begin{aligned} \tilde{H}'_{AKLT} = \sum_{j=1}^L d_j \left[ \mathbf{S}_j \cdot \mathbf{S}_{j+1} + \mathbf{S}_{j+1} \cdot \mathbf{S}_{j+2} \right. \\ \left. + \frac{1}{2} \mathbf{S}_j \cdot \mathbf{S}_{j+2} - \frac{1}{2} (\mathbf{S}_j \cdot \mathbf{S}_{j+2})^2 + 3 \right], \end{aligned} \quad (32)$$

where each coefficient  $d_j$  can be any real number. This means that adding this term to the Hamiltonian  $\tilde{H}(t)$  in Eq. (30) leaves the scar state unaffected. Second, we consider higher-order conserved charges  $Q_{2k+1}$  ( $k > 1$ ) of the SU(3) Sutherland model, whose explicit expressions can be found in Ref. [65]. Since the VBS state is an integrable boundary state, it is annihilated by all  $Q_{2k+1}$  (see Appendix C). Thus, adding these terms with arbitrary coefficients does not affect the scar state. Combining these two generalizations leads to the following Hamiltonian:

$$\tilde{H}(t_1, t_2, \dots, t_n) = \tilde{H}(t_1) + \tilde{H}'_{AKLT} + \sum_{k=2}^n t_k Q_{2k+1}, \quad (33)$$

in which the VBS state survives as a scar state.

Let us finally discuss higher-spin generalizations. The spin-1 AKLT model can be generalized to models with SO(5) and more generally SO( $2l + 1$ ) symmetry [102–104]. The exact ground states of these models, which we dub SO( $2l + 1$ ) VBS states, take the form of a matrix product state built from  $2l + 1$  gamma matrices. According to the general theory of integrable boundary states [61], the SO( $2l + 1$ ) VBS state is an integrable boundary state of the SU( $2l + 1$ ) Heisenberg model, meaning that the state is annihilated by all parity-odd conserved charges of the model. Thus, the construction of deformed models proceeds in much the same way as in the SU(2) case. We also note that the parent Hamiltonian of the SO( $2l + 1$ ) VBS state can be inhomogeneous, like the one in Eq. (31). We thus expect that the models constructed in this way are nonintegrable for general  $l$  and can be thought of as scarred models.

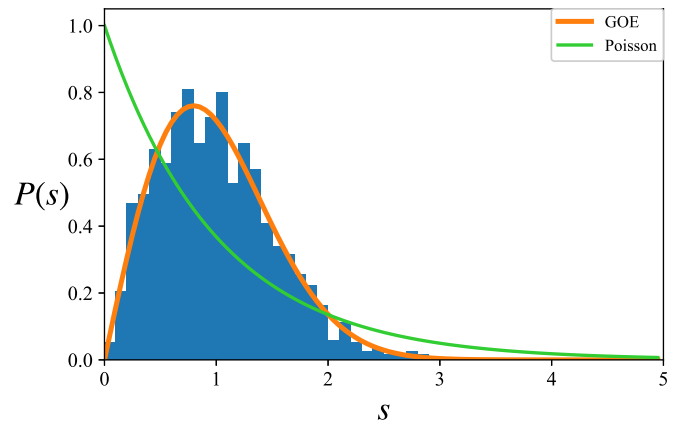


FIG. 12. Level-spacing statistics in the middle half of the spectrum of the model (34) with  $t = 3$  and  $L = 13$ . The data are taken in the symmetry sector where  $(\mathcal{S}^z, \mathcal{S}, \mathcal{T}, \mathcal{F}) = (0, 0, 1, 1)$ . The curves  $P(s)_{GOE}$  (orange) and  $P(s)_{Poisson}$  (green) are shown for comparison. The distribution follows  $P(s)_{GOE}$ .

## V. SPIN-1 AKLT MODEL + SCALAR SPIN CHIRALITY

The model considered in this section is an example of a scarred model constructed by method (ii) with  $n = 0$  mentioned in Sec. II A.

### A. Hamiltonian

In this section, we consider another spin-1 model in which the VBS state in Eq. (24) is a scar state. The Hamiltonian of the model is given by

$$H(t) = H_{AKLT} + t C_{SC}, \quad (34)$$

where  $H_{AKLT}$  is the AKLT Hamiltonian in Eq. (18), and

$$C_{SC} = \sum_{j=1}^L \mathbf{S}_j \cdot (\mathbf{S}_{j+1} \times \mathbf{S}_{j+2}), \quad (35)$$

is the scalar spin chirality term with  $\mathbf{S}_j$  being the spin-1 operators in Eq. (16).

This model has the same symmetries as  $H(t)$  in Eq. (17), i.e., SU(2) spin rotation, translation, spin-flip, and pseudo-time-reversal symmetries. (See Sec. IV for details.) Since the AKLT Hamiltonian is nonintegrable, it is quite likely that the model Eq. (34) is not integrable either. This is indeed the case as can be seen from Fig. 12. Clearly, the level-spacing distribution is close to the GOE Wigner-Dyson distribution. To provide further evidence for this, we compute the  $r$  value from the histogram and obtain  $\langle r \rangle \simeq 0.536$ , which agrees with  $\langle r_{GOE} \rangle \simeq 0.536$ .

### B. Scar state

The VBS state  $|\Psi_{VBS}\rangle$  in Eq. (24) is the zero-energy ground state of  $H_{AKLT}$ . Interestingly, one can show that  $|\Psi_{VBS}\rangle$  is an eigenstate of  $C_{SC}$  with eigenvalue 0 using its matrix product state representation (see Appendix E for a proof). Thus,  $|\Psi_{VBS}\rangle$  is a simultaneous eigenstate of  $H_{AKLT}$  and  $C_{SC}$ , and is likely to be a scar state of the system. We checked it by computing half-chain entanglement entropies (Fig. 13). The

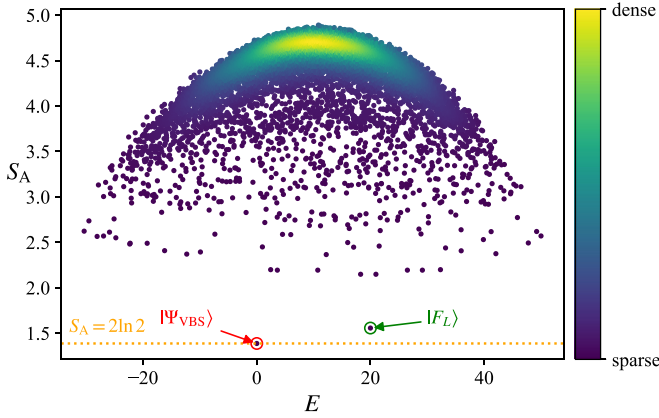


FIG. 13. Entanglement entropies in all eigenstates of  $H(t)$  in Eq. (34) with  $t = 3$  for  $L = 10$  in the  $S^z = 0$  sector. The density of data points is color coded. The red and green circles indicate the VBS and ferromagnetic states, respectively. The orange dotted line indicates  $S_A = 2 \ln 2 \simeq 1.386$ .

obtained results show that the VBS state has sufficiently low entanglement entropy compared to other states, confirming that it is indeed nonthermal.

## VI. PERTURBED SPIN-1 SCALAR SPIN CHIRALITY

In this section, we consider a class of Hamiltonians consisting of the spin-1 scalar spin chirality term  $C_{SC}$  in Eq. (35) and some other terms. They are examples of models constructed by method (ii) discussed in Sec. II A. To provide some insight into what is special about this class of models, we have calculated the half-chain entanglement entropies in all eigenstates of the Hamiltonian

$$H_0(h) = C_{SC} + h \sum_{j=1}^L S_j^z, \quad (36)$$

for  $h = 1$  and  $L = 8$ . The results in Fig. 14 indicate towers of low-entanglement states forming multiple arcs bridging  $E = \pm 8$ , but it is hard to distinguish them clearly because of degeneracies due to additional symmetries. In the following subsections, we classify these eigenstates and remove the degeneracies by introducing extra inhomogeneous terms.

### A. Zero-energy states of $C_{SC}$

Interestingly, one can explicitly construct some zero-energy states of  $C_{SC}$  by acting with certain ladder operators on reference states  $|\uparrow\rangle := |+\cdots+\rangle$  and  $|\mathbf{0}\rangle := |00\cdots 0\rangle$ , where  $|+\rangle$ ,  $|0\rangle$ , and  $|-\rangle$  are eigenstates of  $S^z$  with eigenvalues  $+1$ ,  $0$ , and  $-1$ , respectively. We define the ladder operators by

$$\mathcal{O}_p^- = \sum_{j=1}^L e^{ipj} S_j^-, \quad \mathcal{Q}_p^- = \sum_{j=1}^L e^{ipj} (S_j^-)^2, \quad (37)$$

where  $S_j^- = S_j^x - iS_j^y$ . The subscript  $p$  indicates that the operator carries momentum  $p$ , which takes the values  $p = \frac{2\pi n}{L}$

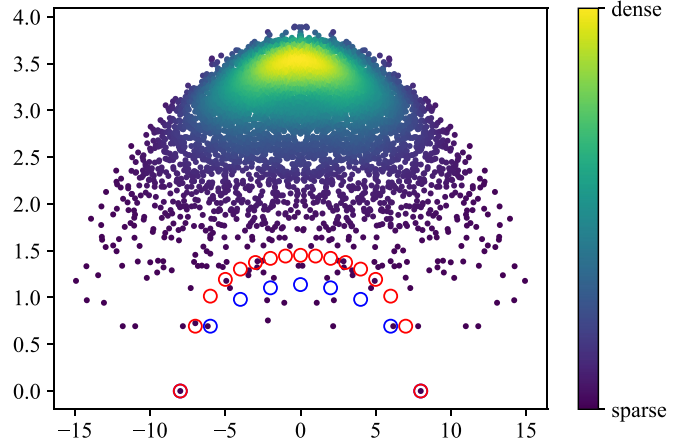


FIG. 14. Entanglement entropies in all eigenstates of (36) for  $L = 8$ ,  $h = 1$ . The density of data points is color coded. The red and blue circles indicate the positions of  $|A_{0,n}\rangle$  in Eq. (38) and  $|B_{0,n}\rangle$  in Eq. (39), respectively.

with  $n = 0, 1, \dots, L - 1$ . We find that the following states are zero-energy states of  $C_{SC}$ :

$$|A_{m,n}\rangle := (\mathcal{O}_0^-)^m (\mathcal{O}_\pi^-)^n |\uparrow\rangle \quad (0 \leq m + n \leq 2L), \quad (38)$$

$$|B_{m,n}\rangle := (\mathcal{O}_0^-)^m (\mathcal{Q}_0^-)^n |\uparrow\rangle \quad (n \geq 1, 1 \leq m \leq 2L - 2n). \quad (39)$$

Note that  $|A_{m,n}\rangle$  are well defined only for even  $L$ . To see that the above states are zero-energy states of  $C_{SC}$ , it suffices to consider the case  $m = 0$ . This is because the operator  $\mathcal{O}_0^-$  is exactly the spin-lowering operator  $\mathcal{S}^- = \sum_{j=1}^L S_j^-$  commuting with  $C_{SC}$  due to the  $SU(2)$  symmetry. For convenience, we introduce the notation  $|\bar{A}_n\rangle := |A_{0,n}\rangle$ ,  $|\bar{B}_n\rangle := |B_{0,n}\rangle$  to denote the above states with  $m = 0$ . One can prove that  $|\bar{A}_n\rangle$  and  $|\bar{B}_n\rangle$  are zero-energy eigenstates of  $C_{SC}$  by noting that  $C_{SC}$  and either  $\mathcal{O}_\pi^-$  or  $\mathcal{Q}_0^-$  satisfy a restricted spectrum generating algebra of order 2 [62]. See Appendix F for the proof.

The towers of states  $|A_{m,n}\rangle$  and  $|B_{m,n}\rangle$  do not exhaust the zero-energy manifold of  $C_{SC}$ . In fact, there are other towers of zero-energy states generated by  $\mathcal{O}_p^-$ ,

$$|+\rangle_m := (\mathcal{O}_0^+)^m |\mathbf{0}\rangle, \quad (40)$$

$$|-\rangle_m := (\mathcal{O}_0^-)^m |\mathbf{0}\rangle, \quad (41)$$

$$|K_{m,p}\rangle := (\mathcal{O}_0^-)^m \mathcal{O}_p^- \mathcal{O}_{-p}^- |\uparrow\rangle, \quad (42)$$

where  $0 \leq m \leq 2L - 2$  and  $p = \frac{2\pi}{L}, \frac{4\pi}{L}, \dots, \frac{2\pi}{L} (\lfloor \frac{L}{2} \rfloor - 1)$ . Again since  $\mathcal{O}_0^-$  commutes with  $C_{SC}$ , it suffices to consider the case  $m = 0$ . It is easy to see that  $|+\rangle_0 = |-\rangle_0 = |\mathbf{0}\rangle$  is annihilated by each local term in  $C_{SC}$ , and hence  $C_{SC}|\pm\rangle_0 = 0$ . To see that  $C_{SC}|K_{m,p}\rangle = 0$ , it is convenient to rewrite the state  $|K_{0,p}\rangle$  as

$$|K_{0,p}\rangle = \sum_{n=1}^L e^{inp} |\Phi_n\rangle \quad (43)$$

where

$$|\Phi_n\rangle = \sum_{j=1}^L S_j^- S_{j+n}^- |\uparrow\rangle. \quad (44)$$

One can show that each  $|\Phi_n\rangle$  is annihilated by  $C_{SC}$ . Therefore, it follows that  $C_{SC}|K_{m,p}\rangle = 0$ . See Appendix F for a detailed proof.

In this way, we have constructed a number of exact zero-energy states of  $C_{SC}$ . It should be noted that they are exact eigenstates of  $H_0(h) = C_{SC} + hS^z$  as well because each of them is a superposition of states with fixed  $S^z$ . We also remark that the obtained states in Eqs. (38)–(42) are not orthogonal to each other. In fact, they are not even linearly independent. This can be seen by considering, for example, the  $L = 3$  site chain. In this case,  $|B_{1,1}\rangle$ ,  $|B_{3,0}\rangle$ , and  $|+_0\rangle$  satisfy  $3|B_{1,1}\rangle - |B_{3,0}\rangle + 12\sqrt{2}|+_0\rangle = 0$ , and hence linearly dependent. In Appendix F, we derive a lower bound on the number of zero-energy states of  $C_{SC}$ , which proves that the number grows exponentially with the system size. Such an exponentially large degeneracy can be a source of QMBS and Hilbert space fragmentation, as discussed in the context of geometrically frustrated systems [105,106].

In the following, we will consider  $H_0(h)$  in Eq. (36) under tailored disorder, which is designed such that some of the obtained zero-energy states of  $C_{SC}$  remain intact.

### B. Random single-ion anisotropy—scarred $|\bar{B}_n\rangle$

In this subsection, we focus on the model in which  $|\bar{B}_n\rangle = (\mathcal{Q}_0^-)^n |\uparrow\rangle$ , ( $n = 1, 2, \dots, L$ ) become scars. We consider the Hamiltonian

$$H_1(h, \{D_j\}_j) = C_{SC} + h \sum_{j=1}^L S_j^z + \sum_{j=1}^L D_j (S_j^z)^2, \quad (45)$$

where  $D_j$  are any real numbers. In what follows, we omit the dependence of  $H_1$  on  $h$  and  $\{D_j\}_j$  unless necessary.

Since  $H_1$  commutes with  $S^z$ , one can split the Hilbert space into subspaces labeled by the eigenvalues of  $S^z$ . The  $S^z = 0$  subspace is special in that it is invariant under spin flip  $\mathcal{F}$ . Thus, this subspace can be further divided into two sectors: one with  $\mathcal{F} = 1$  and the other with  $\mathcal{F} = -1$ . We have analyzed the level-spacing statistics in the sector  $(S^z, \mathcal{F}) = (0, 1)$  and found that the distribution is close to the GUE Wigner-Dyson distribution. We also calculated the  $r$  value and obtained  $\langle r \rangle \simeq 0.593$ , which is consistent with the GUE.

#### 1. Tower of eigenstates

The states  $|\bar{B}_n\rangle$  constitute a tower of eigenstates of  $H_1$ . This can be seen as follows. In the previous subsection, we have already shown that each  $|\bar{B}_n\rangle$  is a simultaneous eigenstate of  $C_{SC}$  and  $S^z$ . Thus it remains to show that these states are eigenstates of the third term on the RHS of Eq. (45), which we call the  $D$  term. To show this, we take a closer look at  $|\bar{B}_n\rangle$ . In the basis of  $S_j^z$  eigenstates, they read

$$|\bar{B}_0\rangle = |\uparrow\rangle = |+\cdots+\rangle, \quad (46)$$

:

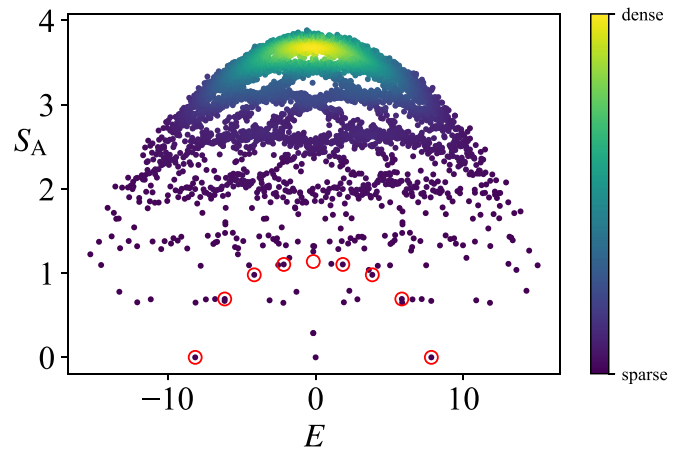


FIG. 15. Entanglement entropies in all eigenstates of  $H_1(h, \{D_j\})$  in Eq. (45) for  $L = 8, h = 1, D_j \in [-1, 1]$ . The density of data points is color coded. The red circle corresponds to  $|\bar{B}_n\rangle$  ( $n = 0, 1, \dots, L$ ).

$$|\bar{B}_n\rangle = (\mathcal{Q}_0^-)^n |\uparrow\rangle = 2^n \times n! \sum_{1 \leq j_1 < j_2 < \dots < j_n \leq L} |+\cdots -_{j_1} \cdots -_{j_2} \cdots -_{j_n} \cdots +\rangle, \quad (47)$$

:

$$|\bar{B}_L\rangle = 2^L \times L! |-\cdots-\rangle. \quad (48)$$

As one can see, each  $|\bar{B}_n\rangle$  consists of sequences of  $|\pm\rangle$ , in which the state  $|0\rangle$  never appears. Therefore, each  $|\bar{B}_n\rangle$  is an eigenstate of  $(S_j^z)^2$  with eigenvalue 1 for all  $j$ , implying that  $|\bar{B}_n\rangle$  is an eigenstate of the  $D$  term with eigenvalue  $\sum_j D_j$ .

One can calculate the half-chain entanglement entropy of  $|\bar{B}_n\rangle$  in the same way as the ferromagnetic states with spin-1/2. The result reads

$$S_A(|\bar{B}_n\rangle) = - \sum_{k=0}^n \frac{\binom{L/2}{k} \binom{L/2}{n-k}}{\binom{L}{n}} \ln \frac{\binom{L/2}{k} \binom{L/2}{n-k}}{\binom{L}{n}}. \quad (49)$$

(see Appendix A for details). The state  $|\bar{B}_{L/2}\rangle$  has the largest entanglement entropy in  $\{|\bar{B}_n\rangle\}_{n=0,1,\dots,L}$ , and the asymptotic form of  $S_A(|\bar{B}_{L/2}\rangle)$  for  $L \gg 1$  is given by

$$S_A(|\bar{B}_{L/2}\rangle) \approx \frac{1}{2} \left( \ln \frac{\pi L}{8} + 1 \right), \quad (50)$$

which obeys a sub-volume law.

Figure 15 shows the half-chain entanglement entropy as a function of energy for  $H_1$  with  $L = 8, h = 1$ , and  $D_j$  randomly chosen from  $[-1, 1]$ . As one can see, the states  $|\bar{B}_n\rangle$  form a tower of low-entanglement states. They are, however, not well separated from other states due to the presence of other low-entanglement states. The obtained result also suggests that the energy  $E = 0$  is highly degenerate even in the presence of disorder in  $D_j$ . Since we obtain superpositions of degenerate eigenstates in numerical diagonalization, the entanglement entropy of the state  $|\bar{B}_{L/2}\rangle$  at this energy is obscured. This may be the reason why a data point is missing in the red circle at  $E = 0$ .

In order to resolve the degeneracy, we now consider the sector with fixed quantum numbers  $(S^z, \mathcal{F}) = (0, 1)$ .

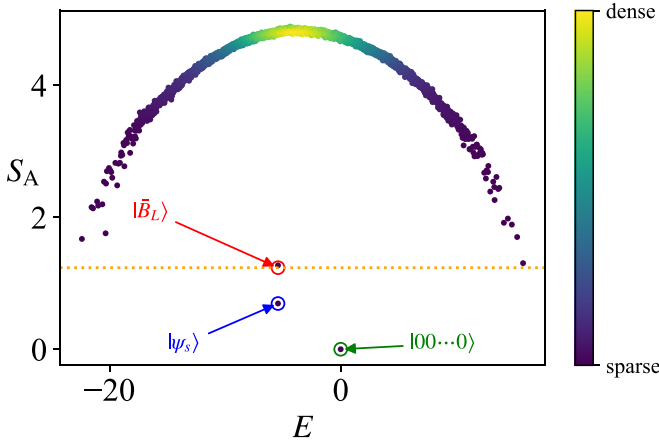


FIG. 16. Entanglement entropies in all eigenstates of  $H_1(h, \{D_j\})$  in Eq. (45) for  $L = 10$ ,  $h = 1$  in the symmetry sector  $(S^z, \mathcal{F}) = (0, 1)$ . Each  $D_j$  is randomly chosen from  $[-5, 5]$ . The density of data points is color coded. The entanglement entropy of each state obeys a volume-law except for  $|\bar{B}_{L/2}\rangle$ , the symmetric state  $|\psi_s\rangle = |+-+\dots\rangle + |-+-+\dots\rangle$ , and the trivial state  $|\mathbf{0}\rangle = |00\dots 0\rangle$ . The orange dotted line indicates  $S_A = 1.236$ , which is obtained from Eq. (49) for  $L = 10$ .

Figure 16 shows the entanglement entropies of the eigenstates of  $H_1$  in this symmetry sector. Clearly, the state  $|\bar{B}_{L/2}\rangle$  is isolated from the other states, indicating its nonthermal nature. In addition to this state, there are two other entropy outliers:  $|\psi_s\rangle = |+-+\dots\rangle + |-+-+\dots\rangle$  and  $|\mathbf{0}\rangle$ . These states are zero-energy states of  $C_{SC}$  that remain intact under the influence of the  $D$  term. However,  $|\mathbf{0}\rangle$  cannot be thought of as a scar. This is because the projection onto this state, namely  $\mathcal{P} = \prod_{j=1}^L (1 - S_j^z)^2$ , commutes with the Hamiltonian  $H_1$ , which simply means that  $|\mathbf{0}\rangle$  is the state that is uniquely specified by the eigenvalue 1 of  $\mathcal{P}$ . Thus, out of the three entropy outliers, only  $|\bar{B}_{L/2}\rangle$  and  $|\psi_s\rangle$  are identified as QMBS. Figure 17 shows the expectation values of a local observable for all eigenstates of  $H_1$  in the sector with  $(S^z, \mathcal{F}) = (0, 1)$ . As an observable, we consider  $H_{AKLT}$  in Eq. (18). As we can see, the expectation values in these three states are isolated from other thermal states, which implies a violation of strong ETH.

## 2. Dynamics

To illustrate the nonthermal features of scarred states, we study the quench dynamics of the system. The initial states we consider are coherent states of  $Q_0^-$ , namely superpositions of  $|\bar{B}_n\rangle$  defined as

$$|\beta\rangle := C_L^{-1} \exp(\beta Q_0^-) |\uparrow\rangle = C_L^{-1} \sum_{n=0}^L \frac{\beta^n}{n!} |\bar{B}_n\rangle, \quad (51)$$

where  $\beta \in \mathbb{C}$  and  $C_L := (1 + 4|\beta|^2)^{\frac{L}{2}}$  is a normalization factor such that  $\langle\beta|\beta\rangle = 1$ . Under time evolution by the Hamiltonian (45), the initial state  $|\beta\rangle$  evolves into

$$|\beta(t)\rangle := e^{-iH_1 t} |\beta\rangle \quad (52)$$

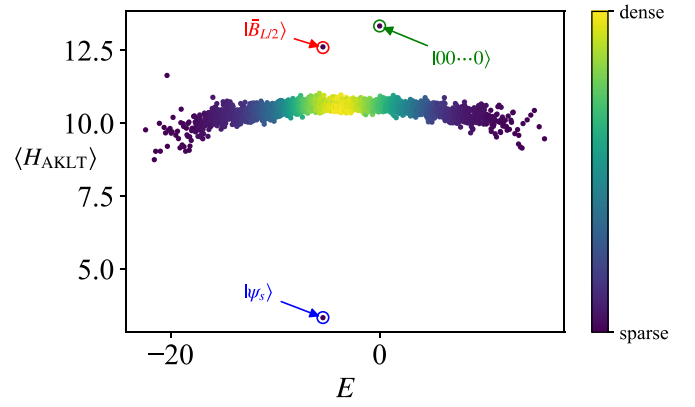


FIG. 17.  $\langle H_{AKLT} \rangle$  in all eigenstates of  $H_1(h, \{D_j\})$  in Eq. (45) for  $L = 10$ ,  $h = 1$  in the symmetry sector  $(S^z, \mathcal{F}) = (0, 1)$ . Each  $D_j$  is randomly chosen from  $[-5, 5]$ . The density of data points is color coded. The red, blue, and green circles indicate  $|\bar{B}_{L/2}\rangle$ ,  $|\psi_s\rangle$ , and  $|00\dots 0\rangle$ , respectively.

at time  $t$ . Since the states  $|\bar{B}_n\rangle$  are common eigenstates of the  $D$  term with eigenvalue  $\mathcal{D} = \sum_j D_j$ , we can rewrite it as

$$|\beta(t)\rangle = e^{-i\mathcal{D}t} e^{-ihS^z t} |\beta\rangle. \quad (53)$$

We first consider the fidelity between initial and time-evolved states. For an arbitrary initial state  $|\phi(0)\rangle$ , it is defined by

$$\mathcal{F}(t) = |\langle\phi(0)|\phi(t)\rangle|, \quad (54)$$

where  $|\phi(t)\rangle = e^{-iH_1 t} |\phi(0)\rangle$ . For the coherent states  $|\beta\rangle$ , we can calculate the fidelity as

$$\begin{aligned} \mathcal{F}(t) &= C_L^{-2} \left| \sum_{m,n=0}^L \frac{(\beta^*)^m \beta^n}{m!n!} \langle \bar{B}_m | e^{-ihS^z t} | \bar{B}_n \rangle \right| \\ &= C_L^{-2} \left| \sum_{n=0}^L \frac{|\beta|^{2n}}{(n!)^2} e^{2ihnt} \langle \bar{B}_n | \bar{B}_n \rangle \right| \\ &= C_L^{-2} \left| \sum_{n=0}^L (4|\beta|^2 e^{2iht})^n \binom{L}{n} \right| \\ &= \left| \frac{1 + 4|\beta|^2 e^{2iht}}{1 + 4|\beta|^2} \right|^L. \end{aligned} \quad (55)$$

Clearly, it is a periodic function with period  $T = \pi/h$ , exhibiting perfect revivals, i.e.,  $\mathcal{F}(t) = 1$  at  $t = nT$  ( $n \in \mathbb{N}$ ), irrespective of the system size. We show in Fig. 18 the numerical results of the fidelity dynamics with several initial states. As we can see, the coherent states show perfectly periodic revivals, indicating that they never thermalize. This is in stark contrast to the fidelity of a generic state, which decays rapidly to zero. We remark that a perfect revival of the initial state after a time of at most  $\mathcal{O}(\text{poly}(L))$ , in general, implies the existence of QMBS [107].

We next examine the time evolution of the half-chain entanglement entropy for several initial states. In the following, we consider the case of even  $L$ . The half-chain entanglement entropy of the coherent state  $|\beta(t)\rangle$  does not evolve in time. In fact, it is always 0. This can be seen by noting that  $|\beta(t)\rangle$  is

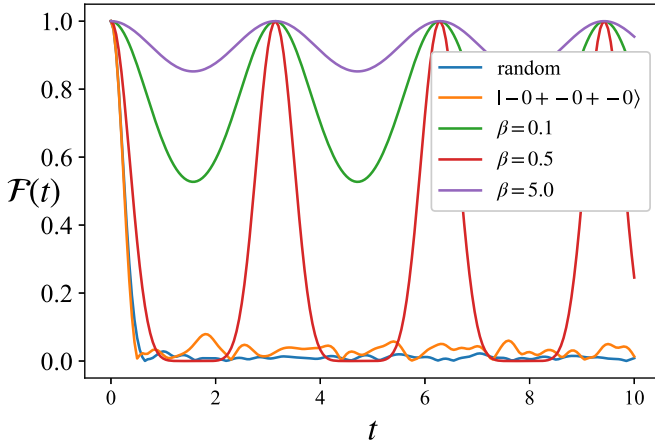


FIG. 18. The dynamics of the fidelity with  $L = 8$ ,  $h = 1$ , and  $D_j$  ( $j = 1, 2, \dots, L$ ) chosen randomly from  $[-1, 1]$ . Perfectly periodic revivals can be seen when the initial state is a coherent state, whereas for other generic states the fidelity decays rapidly to zero.

just a product of two states,

$$|\beta(t)\rangle = e^{-iD_t} e^{-ihS_A^z t} |\beta\rangle_A \otimes e^{-ihS_B^z t} |\beta\rangle_B, \quad (56)$$

where  $S_{A(B)}^z = \sum_{j \in A(B)} S_j^z$  and

$$|\beta\rangle_{A(B)} := C_{L/2}^{-1} \exp\left(\beta \sum_{j \in A(B)} (S_j^-)^2\right) |\uparrow\rangle_{A(B)} \quad (57)$$

with  $|\uparrow\rangle_{A(B)} = \otimes_{j \in A(B)} |+\rangle_j$ . Let us slightly generalize the initial state by considering a superposition of coherent states with different  $\beta$ , namely,  $\sum_{i=1}^n c_i |\beta_i\rangle$ . Since  $|\beta_i\rangle_L = |\beta_i\rangle_A \otimes |\beta_i\rangle_B$ , the entanglement entropy is obtained as [108,109]

$$S_A = -\frac{\text{Tr}[M^2 \ln M^2]}{\text{Tr}[M^2]} + \ln \text{Tr}[M^2], \quad (58)$$

where the matrix elements of  $M$  are defined as

$$M_{i,j} = c_i^* c_j \langle \beta_i | \beta_j \rangle_A = \frac{c_i^* c_j (1 + 4\beta_i^* \beta_j)^N}{(1 + 4|\beta_i|^2)^{\frac{N}{2}} (1 + 4|\beta_j|^2)^{\frac{N}{2}}}. \quad (59)$$

It is then clear that the entanglement entropy for this class of states is constant in time.

Figure 19 shows the time evolution of the half-chain entanglement entropy  $S_A$  for several initial states. Clearly, the coherent states and their superposition do not gain entanglement. By contrast,  $S_A$  of the product state  $|-0+ -0+ -0\rangle$  grows rapidly and saturates near the Page value [110] of a random state

$$S_{\text{Page}} = \frac{L}{2} \ln 3 - \frac{1}{2}. \quad (60)$$

### C. Scarred $|\bar{A}_n\rangle$

#### 1. Tower of eigenstates

As we have seen in the previous subsection, the key to finding a suitable perturbation is to find an operator that acts on a set of target states as a constant. To find such an operator for  $|\bar{A}_n\rangle$ , let us take a closer look at these states. The operator  $\mathcal{O}_\pi^-$  that generates  $|\bar{A}_n\rangle$  is invariant under translation by two sites. Therefore, considering its action on the two neighboring

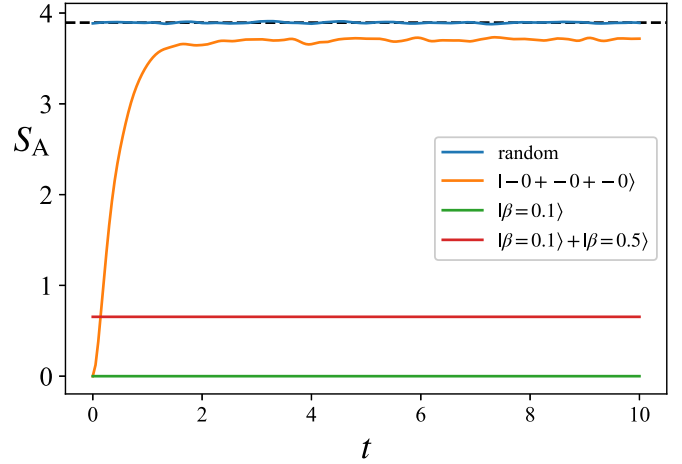


FIG. 19. Dynamics of the half-chain entanglement entropies with the same setup as Fig. 18. The dashed line indicates the Page value  $S_{\text{Page}}$  [Eq. (60)]. Initial coherent states have constant entanglement entropy, but that of  $|-0+ -0+ -0\rangle$  rapidly grows and saturates near  $S_{\text{Page}}$ .

sites may suggest a suitable operator. The operator  $\mathcal{O}_\pi^-$  acts as  $S_j^- - S_{j+1}^-$  at the two neighboring sites ( $j, j+1$ ), and as a result, we get the states listed in Table I by repeatedly applying it to the state  $|+\rangle_{j,j+1}$ .

Each state in the table is a simultaneous eigenstate of  $S_j^z + S_{j+1}^z$  and  $P_{j,j+1}$ , the permutation operator between site  $j$  and  $j+1$  [see Eq. (21)]. From this result, we see that  $(-1)^{S_j^z + S_{j+1}^z} P_{j,j+1} = 1$  holds in the subspace spanned by these states. Therefore, each  $|\bar{A}_n\rangle$  is an eigenstate of the following Hamiltonian:

$$H_2(h, \{D_j\}_j) = C_{\text{sc}} + h \sum_{j=1}^L S_j^z + \sum_{j=1}^L D_j (-1)^{S_j^z + S_{j+1}^z} P_{j,j+1}, \quad (61)$$

where  $D_j$  are any real numbers. One can, in principle, construct a more complicated Hamiltonian involving more than two-spin interactions using the same strategy.

In what follows, we assume that the number of sites  $L$  is even and omit the dependence of  $H_2$  on  $h$  and  $D_j$  unless necessary. Interestingly, the states  $|\bar{B}_n\rangle$  are also eigenstates of  $H_2$  since  $|\bar{B}_n\rangle$  is totally symmetric, i.e.,  $P_{i,j} |\bar{B}_n\rangle = |\bar{B}_n\rangle$  for any  $i, j$  and  $S_j^z + S_{j+1}^z$  is even for any  $j$ . We can see from Fig. 20(a) that the states  $|\bar{A}_n\rangle$  behave as QMBS in this system. On the other hand, the data points for the states  $|\bar{B}_n\rangle$  are mostly missing due to the degeneracies.

TABLE I. The explicit form of  $(S_j^- - S_{j+1}^-)^n |+\rangle_{j,j+1}$  up to constant factors. The third and fourth columns indicate the eigenvalues of the corresponding operators for each state.

$n$	State	$S_j^z + S_{j+1}^z$	$P_{j,j+1}$
0	$ +\rangle$	2	1
1	$ 0+\rangle -  +0\rangle$	1	-1
2	$ -\rangle + 2 00\rangle +  +-\rangle$	0	1
3	$ 0-\rangle -  -0\rangle$	-1	-1
4	$ --\rangle$	-2	1

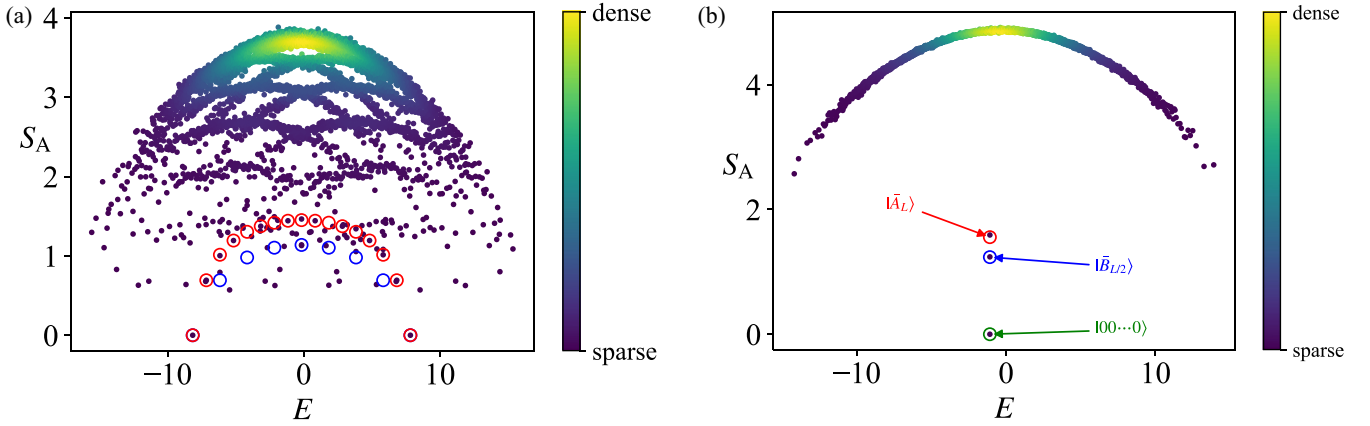


FIG. 20. (a) Entanglement entropies in all eigenstates in Eq. (61) with  $L = 10$ ,  $h = 1$ . Each  $D_j$  is randomly chosen from  $[-1, 1]$ . The density of data points is color coded. The states  $|\bar{A}_n\rangle$  (red circles) and  $|\bar{B}_n\rangle$  (blue circles) have relatively low entanglement entropy. Note that although  $|\bar{A}_n\rangle$  and  $|\bar{B}_n\rangle$  are eigenstates of  $H_2(h, \{D_j\}_j)$ , some circles do not overlap with corresponding data points because of degeneracies. (b) Entanglement entropies in all eigenstates of inhomogeneous model Eq. (61) for  $L = 10$ ,  $h = 1$  in the symmetry sector  $\mathcal{S}^z = 0$ . Each  $D_j$  is randomly chosen from  $[-1, 1]$ . The density of data points is color coded. The red, blue and green circles indicate  $|\bar{A}_L\rangle$ ,  $|\bar{B}_{L/2}\rangle$ , and  $|000\dots 0\rangle$ , respectively.

Since the last term in Eq. (61) does not break  $U(1)$  symmetry associated with  $\mathcal{S}^z$ , we can divide the Hilbert space into subspaces according to the eigenvalues of  $\mathcal{S}^z$ . The  $\mathcal{S}^z = 0$  subspace can be further decomposed into two sectors with opposite  $\mathcal{F}$ . We have analyzed the level-spacing statistics in the sector  $(\mathcal{S}^z, \mathcal{F}) = (0, 1)$  and found that the distribution is close to the GUE Wigner-Dyson distribution. We also calculated the  $r$  value and obtained  $\langle r \rangle \simeq 0.593$ , which is consistent with the GUE.

Figure 20(b) shows the entanglement entropies of eigenstates of  $H_2$  in the sector  $\mathcal{S}^z = 0$ . In the figure, both  $|\bar{A}_L\rangle$  and  $|\bar{B}_{L/2}\rangle$  can be identified as entanglement outliers, which leads us to the conclusion that  $|\bar{B}_n\rangle$  are also QMBS for  $H_2$ . It should be noted that another entanglement outlier, i.e.,  $|0\rangle = |000\dots 0\rangle$  in Fig. 20(b), cannot be thought of as a scar. This is because the projection onto this state, namely  $\mathcal{P} = \prod_{j=1}^L (1 - (\mathcal{S}_j^z)^2)$ , commutes with  $H_2$ , which simply means that this state is uniquely specified by the eigenvalue 1 of  $\mathcal{P}$ .

## 2. Dynamics

Similarly to the previous subsection, we introduce a coherent state of  $\mathcal{O}_\pi$ , namely a superposition of  $|\bar{A}_n\rangle$  defined by

$$|\alpha\rangle = \tilde{C}_L^{-1} \exp(\alpha \mathcal{O}_\pi^-) |\uparrow\rangle = \tilde{C}_L^{-1} \sum_{n=0}^{2L} \frac{\alpha^n}{n!} |\bar{A}_n\rangle, \quad (62)$$

where  $\tilde{C}_L = (1 + |\alpha|^2)^L$  is the normalization constant. When the initial state is the coherent state  $|\alpha\rangle$ , the fidelity defined in Eq. (54) can be computed as

$$\begin{aligned} \mathcal{F}(t) &= \tilde{C}_L^{-2} \left| \sum_{m,n=0}^{2L} \frac{\alpha^{*m} \alpha^n}{m!n!} \langle \bar{A}_m | e^{-iH_2 t} | \bar{A}_n \rangle \right| \\ &= \tilde{C}_L^{-2} \left| \sum_{n=0}^{2L} \frac{|\alpha|^{2n}}{(n!)^2} e^{ihn t} \langle \bar{A}_n | \bar{A}_n \rangle \right| \end{aligned}$$

$$\begin{aligned} &= \tilde{C}_L^{-2} \left| \sum_{n=0}^{2L} (|\alpha|^2 e^{ihn})^n \binom{2L}{n} \right| \\ &= \left| \frac{1 + |\alpha|^2 e^{ihn}}{1 + |\alpha|^2} \right|^{2L}. \end{aligned} \quad (63)$$

Thus, it attains the maximum fidelity  $\mathcal{F}(t) = 1$  periodically with period  $T = 2\pi/h$ . Figure 21 shows the numerical results of the fidelity dynamics with several initial states. Here we set  $h = 1$ . Clearly, the coherent states attain  $\mathcal{F}(t) = 1$  periodically with period  $2\pi$ , whereas the fidelities of the other states decay rapidly to zero. We also calculated the time evolution of the entanglement entropy for these states and obtained a result similar to that shown in Fig. 19. See Appendix G for the dynamics from a more complex initial state.

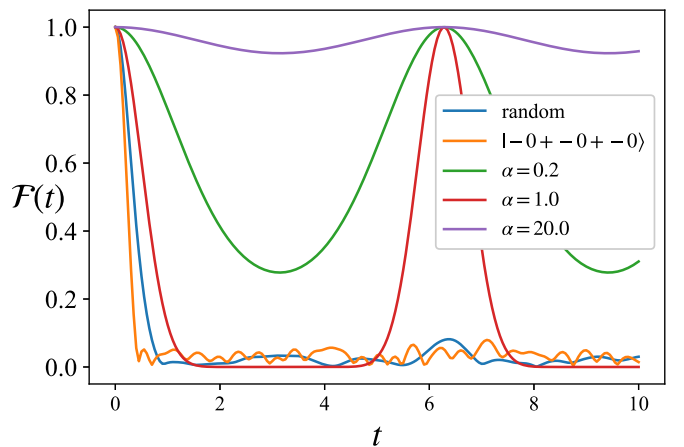


FIG. 21. The dynamics of the fidelity with  $h = 1$ ,  $L = 8$ , and  $D_j$  ( $j = 1, 2, \dots, L$ ) chosen randomly from  $[-1, 1]$ . The fidelity shows perfectly periodic revivals when the initial state is a coherent state, whereas it decays rapidly to zero for other generic states.

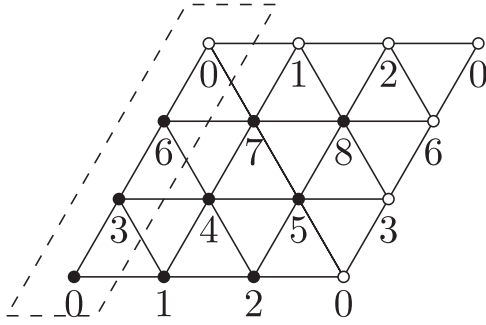


FIG. 22. An example of the triangular lattice. The integers denote the site indices, and the black and white sites with the same index are identified by the periodic boundary conditions. We take the subsystem  $A$  to be the set of sites enclosed by the dashed lines, which is used to calculate the entanglement entropy.

#### D. Two-dimensional model

In the same way as before, we can construct two-dimensional models with QMBS. Here we consider the generalization of the model  $H_1$  in Eq. (45) on a triangular lattice with periodic boundary conditions (Fig. 22). Let  $\Lambda$  be the triangular lattice. The Hamiltonian is

$$H_1^{2d}(h, \{D_j\}_j) = C_{SC}^{2d} + h \sum_{j \in \Lambda} S_j^z + \sum_{j \in \Lambda} D_j (S_j^z)^2, \quad (64)$$

where

$$C_{SC}^{2d} = \sum_{\Delta/\nabla} \mathbf{S}_j \cdot (\mathbf{S}_k \times \mathbf{S}_l), \quad (65)$$

and the summation is over all triangles. The subscripts  $j, k$ , and  $l$  are in the clockwise (counterclockwise) order in each upward (downward) triangle.

Analogously to the states  $|\bar{B}_n\rangle$ , one can define the following states:

$$|\Psi_n\rangle = (\mathcal{Q}_0^-)^n |\uparrow\rangle = \left( \sum_{j \in \Lambda} (S_j^-)^2 \right)^n |\uparrow\rangle. \quad (66)$$

Since  $\mathcal{Q}_0^-$  can be decomposed into  $\mathcal{Q}_0^- = \mathcal{Q}_X + \mathcal{Q}_{\Lambda \setminus X}$  with  $\mathcal{Q}_X := \sum_{i \in X} (S_i^-)^2$  and  $\mathcal{Q}_{\Lambda \setminus X} := \mathcal{Q}_0^- - \mathcal{Q}_X$  for any  $X = \{j, k, l\}$  forming an upward or downward triangle, we obtain

$$|\Psi_n\rangle = \sum_{p=0}^n \binom{n}{p} (\mathcal{Q}_X)^p |++\rangle_X \otimes (\mathcal{Q}_{\Lambda \setminus X})^{n-p} |++\dots+\rangle_{\Lambda \setminus X}. \quad (67)$$

Then, one can show that  $\mathbf{S}_j \cdot (\mathbf{S}_k \times \mathbf{S}_l) (\mathcal{Q}_X)^p |++\rangle_X = 0$  for any  $X$  and  $p$  in the same way as in the one-dimensional case. Therefore,  $|\Psi_n\rangle$  is an eigenstate of  $C_{SC}^{2d}$  with eigenvalue 0. Furthermore, since  $D_j (S_j^z)^2$  acts only on one site,  $D_j (S_j^z)^2 |\Psi_n\rangle = D_j |\Psi_n\rangle$  can be shown in the same way as in the one-dimensional case. Therefore, each  $|\Psi_n\rangle$  is an eigenstate of  $H_1^{2d}$  in Eq. (64) with eigenvalue  $h(|\Lambda| - 2n) + \sum_{j=1}^L D_j$ , where by  $|\Lambda|$  we denote the total number of sites in  $\Lambda$ .

To see whether  $|\Psi_n\rangle$  are QMBS, we calculate entanglement entropies in all eigenstates of  $H_1^{2d}$  in the symmetry sector with  $S^z = 1$ . In the calculation, we take the subsystem  $A$  to

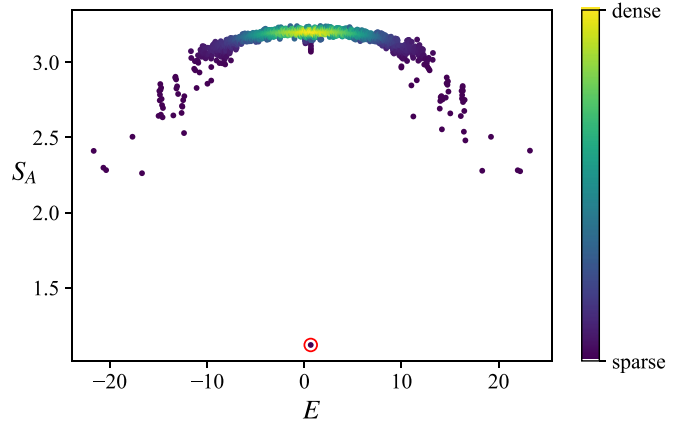


FIG. 23. Entanglement entropies in all eigenstates of  $H_1^{2d}(h, \{D_j\})$  in Eq. (64) for  $L = 9, h = 1$  in the symmetry sector  $S^z = 1$ . Each  $D_j$  is randomly chosen from  $[-1, 1]$ . The density of data points is color coded. The red circle indicates the scar state  $|\Psi_{n=4}\rangle$ .

be  $\{0, 3, 6\}$  (see Fig. 22 for the site labels). As shown in Fig. 23, the state  $|\Psi_{n=4}\rangle$  has significantly lower entanglement entropy than the other states, indicating that this state is a scar state. We have also checked numerically that the entanglement entropy of  $|\Psi_n\rangle$  is extremely low regardless of the choice of the subsystem  $A$ .

## VII. DISCUSSION

We have constructed several examples of quantum spin models with two- and three-body interactions that exhibit QMBS using the two different methods: one based on integrable boundary states and the other focusing on towers of states generated by the raising and lowering operators. We demonstrated that the QMBS in the models behave differently from thermal states by comparing their spectral, dynamical, and entanglement properties with those of other typical states. The methods presented in this paper can be used to systematically construct other models with QMBS. For example, using another combination of conserved charges  $\{Q_{2k+1}\}_{k=1,2,\dots}$  in the first method, one can construct a family of new models in which an integrable boundary state is an exact zero-energy state. The second method discussed in Sec. II is a variant of existing methods, and in particular, it is similar to that of Tang *et al.* [47], where the authors constructed models with towers of scar states generated by irreducible tensor operators. However, their main focus is on spin-1/2 systems, whereas our paper is primarily concerned with spin-1 systems. Moreover, we demonstrated that our method allows for the construction of a two-dimensional model with QMBS.

In future research, it would be interesting to construct nonintegrable models that have multiple integrable boundary states as QMBS. To this end, we need to find a nonintegrable Hamiltonian in which these integrable boundary states become degenerate. Since the idea of integrable boundary states can be traced back to those of integrable quantum field theories [111], it would also be interesting to construct nonintegrable quantum field theories with QMBS by extending our method. In this regard, we note that QMBS in

continuous models have also been discussed in previous studies [112–115].

Another direction worth investigating is to apply our methods to open quantum and periodically driven systems. Previous studies have shown that there are some open or driven systems that fail to thermalize at late times [63, 116–119], where algebraic approaches were also widely used. Finally, it would also be interesting to extend the notion of integrable boundary states to such systems and construct models exhibiting nonthermalizing dynamics. In this respect, dissipative systems described by integrable Lindblad superoperators [120–122] and integrable Floquet systems [123–125] may serve as a good starting point for constructing concrete examples.

### ACKNOWLEDGMENTS

We thank Eric Vernier for valuable discussions and for allowing us to include his proof of Theorem F.1, and Kensuke Tamura for useful discussions. The numerical calculations of the entanglement entropy and the level-spacing statistics were performed using QuSpin [126, 127]. H.K. was supported by MEXT KAKENHI Grant-in Aid for Transformative Research Areas A “Extreme Universe” Grant No. JP21H05191. H.K. was also supported in part by JSPS KAKENHI Grants No. JP18K03445, No. JP23H01093, and the Inamori Foundation. K.S. acknowledges the support of the Forefront Physics and Mathematics Program to Drive Transformation. Y.M. acknowledges the support from the GGI BOOST Fellowship.

### APPENDIX A: ENTANGLEMENT ENTROPY OF THE FERROMAGNETIC STATES

We consider the general spin- $\sigma$  case ( $\sigma = 1/2, 1, 3/2, \dots$ ). The basis states  $|\zeta\rangle$  ( $\zeta = \sigma, \sigma - 1, \dots, -\sigma + 1, -\sigma$ ) on each site are defined such that  $S^z|\zeta\rangle = \zeta|\zeta\rangle$  and  $S^\pm|\zeta\rangle = \sqrt{\sigma(\sigma \pm 1) - \zeta(\zeta \pm 1)}|\zeta \pm 1\rangle$ . We denote the fully polarized state, i.e.,  $|\sigma\rangle^{\otimes L}$  by  $|\uparrow\rangle_L$ . Then the ferromagnetic states as the SU(2) descendants of  $|\uparrow\rangle_L$  are defined as

$$|F_n\rangle_L = \frac{1}{\sqrt{\mathcal{N}_\sigma(n, L)}}(S^-)^n|\uparrow\rangle_L, \quad n = 0, 1, \dots, 2\sigma L \quad (\text{A1})$$

where  $\mathcal{N}_\sigma(n, L)$  is a normalization constant such that  $\langle F_n|F_n\rangle_L = 1$ . One can show that

$$\mathcal{N}_\sigma(n, L) = \frac{n!(2\sigma L)!}{(2\sigma L - n)!} \quad (\text{A2})$$

for all  $\sigma, L$ , and  $n$  using  $[S^+, S^-] = 2S^z$  and the mathematical induction on  $n$ . The proof goes as follows.

First, it is obvious that  $\|(S^-)^0|\uparrow\rangle_L\|^2 = \||\uparrow\rangle_L\|^2 = 1$ . On the other hand, we obtain  $\frac{0!2\sigma L!}{(2\sigma L - 0)!} = 1$ . Thus, Eq. (A2) is valid for  $n = 0$ . Next, we assume Eq. (A2) is true for  $n = k$ . Then we can calculate  $\mathcal{N}_\sigma(k + 1, L)$  as

$$\mathcal{N}_\sigma(k + 1, L) = \langle \uparrow | (S^+)^{k+1} (S^-)^{k+1} | \uparrow \rangle_L \quad (\text{A3})$$

$$= \langle \uparrow | (S^+)^k (S^- S^+ + 2S^z) (S^-)^k | \uparrow \rangle_L \quad (\text{A4})$$

$$= 2(\sigma L - k)\mathcal{N}_\sigma(k, L) + \langle \uparrow | (S^+)^k S^- (S^- S^+ + 2S^z) (S^-)^{k-1} | \uparrow \rangle_L \quad (\text{A5})$$

= ...

$$= 2\{(\sigma L - k) + (\sigma L - k + 1) + \dots + \sigma L\}\mathcal{N}_\sigma(k, L) \quad (\text{A6})$$

$$= \frac{(k + 1)!(2\sigma L)!}{(2\sigma L - (k + 1))!} \quad (\text{A7})$$

Thus, Eq. (A2) is true for  $n = k + 1$ . Hence Eq. (A2) is true for all  $n = 0, 1, \dots, 2\sigma L$ .

To compute the entanglement entropy, we divide the whole chain into two subsystems,  $A$  and  $B$ , with lengths  $L_A$  and  $L_B$ , respectively. Since  $S^- = \sum_{j=1}^L S_j^-$  is the sum of single-site operators, we can rewrite  $S^-$  as  $S^- = S_A^- + S_B^-$ , where  $S_A^- = \sum_{j \in A} S_j^-$  and  $S_B^- = \sum_{j \in B} S_j^-$ . Then, we see that  $|F_n\rangle_L$  can be written in the Schmidt decomposition form

$$|F_n\rangle_L = \frac{1}{\sqrt{\mathcal{N}_\sigma(n, L)}}(S_A^- + S_B^-)^n|\uparrow\rangle_L \quad (\text{A8})$$

$$= \sum_{k=0}^n \frac{1}{\sqrt{\mathcal{N}_\sigma(n, L)}} \binom{n}{k} (S_A^-)^k (S_B^-)^{n-k} |\uparrow\rangle_L \quad (\text{A9})$$

$$= \sum_{k=0}^n \sqrt{\frac{\mathcal{N}_\sigma(k, L_A)\mathcal{N}_\sigma(n-k, L_B)}{\mathcal{N}_\sigma(n, L)}} \times \binom{n}{k} |F_k\rangle_{L_A} \otimes |F_{n-k}\rangle_{L_B}, \quad (\text{A10})$$

from which the entanglement entropy is obtained as

$$S_A(|F_n\rangle_L) = - \sum_{k=0}^n \frac{\mathcal{N}_\sigma(k, L_A)\mathcal{N}_\sigma(n-k, L_B)}{\mathcal{N}_\sigma(n, L)} \binom{n}{k}^2 \times \ln \frac{\mathcal{N}_\sigma(k, L_A)\mathcal{N}_\sigma(n-k, L_B)}{\mathcal{N}_\sigma(n, L)} \binom{n}{k}^2 \quad (\text{A11})$$

$$= - \sum_{k=0}^n \binom{2\sigma L}{n}^{-1} \binom{2\sigma L_A}{k} \binom{2\sigma L_B}{n-k} \times \ln \left[ \binom{2\sigma L}{n}^{-1} \binom{2\sigma L_A}{k} \binom{2\sigma L_B}{n-k} \right]. \quad (\text{A12})$$

We now discuss the asymptotic behavior of  $S_A(|F_n\rangle_L)$  for large  $L$ . In particular, we consider the case where  $L$  is even,  $L_A = L_B = L/2$ , and  $n = \sigma L$ . In this case, one can rewrite Eq. (A8) as

$$S_A(|F_{\sigma L}\rangle_L) = - \sum_{k=0}^{\sigma L} \binom{2\sigma L}{\sigma L}^{-1} \binom{\sigma L}{k}^2 \ln \binom{2\sigma L}{\sigma L}^{-1} \binom{\sigma L}{k}^2 \quad (\text{A13})$$

$$= \binom{2\sigma L}{\sigma L}^{-1} \sum_{k=0}^{\sigma L} \left[ \binom{\sigma L}{k}^2 \ln \binom{2\sigma L}{\sigma L} - \binom{\sigma L}{k}^2 \ln \binom{\sigma L}{k}^2 \right]. \quad (\text{A14})$$

Using the Vandermonde identity, we can rewrite the first term in the bracket as

$$\sum_{k=0}^{\sigma L} \binom{\sigma L}{k}^2 \ln \binom{2\sigma L}{\sigma L} = \binom{2\sigma L}{\sigma L} \ln \binom{2\sigma L}{\sigma L}. \quad (\text{A15})$$

On the other hand, we cannot directly compute the second term for finite  $L$ . However, in the large- $L$  limit, the dominant contribution to the summation comes from large  $k$ . Thus, we can apply the de Moivre-Laplace theorem and evaluate  $\binom{n}{k}$  as

$$\binom{n}{k} = \frac{2^n}{\sqrt{\frac{1}{2}n\pi}} \exp\left[-\frac{2(k-\frac{n}{2})^2}{n}\right] \times \left(1 + \mathcal{O}\left(\frac{1}{\sqrt{n}}\right)\right) \quad (\text{A16})$$

in the limit  $n \rightarrow \infty$  [85,128–130]. Using this asymptotic expansion and the Vandermonde identity, we have

$$\sum_{k=0}^{\sigma L} \binom{\sigma L}{k}^2 \ln \binom{\sigma L}{k}^2 = \binom{2\sigma L}{\sigma L} \left[ 2\sigma L \ln 2 - 2 \ln \sqrt{\frac{\pi\sigma L}{2}} - \frac{\sigma L}{2\sigma L - 1} + \mathcal{O}\left(\frac{1}{\sqrt{L}}\right) \right]. \quad (\text{A17})$$

Substituting this and Eq. (A15) into Eq. (A14), we find

$$S_A(|F_{\sigma L}\rangle_L) = \ln \binom{2\sigma L}{\sigma L} + \frac{\sigma L}{2\sigma L - 1} - 2 \left[ \sigma L \ln 2 - \ln \sqrt{\frac{\pi\sigma L}{2}} \right] + \mathcal{O}\left(\frac{1}{\sqrt{L}}\right). \quad (\text{A18})$$

Finally, using Stirling's formula,  $\ln n! = n \ln n - n + \frac{1}{2} \ln n + \frac{1}{2} \ln 2\pi + \mathcal{O}(n^{-1})$ , we get

$$\ln \binom{2\sigma L}{\sigma L} = 2\sigma L \ln 2 - \frac{1}{2} \ln \sigma L - \frac{1}{2} \ln \pi + \mathcal{O}\left(\frac{1}{L}\right), \quad (\text{A19})$$

and hence we obtain the asymptotic form of Eq. (A14) as

$$S_A(|F_{\sigma L}\rangle_L) = \frac{1}{2} \ln \sigma L + \frac{1}{2} \left( \ln \frac{\pi}{4} + 1 \right) + \mathcal{O}\left(\frac{1}{\sqrt{L}}\right) \quad (L \gg 1). \quad (\text{A20})$$

### APPENDIX B: SU(2) SYMMETRY OF $H_3$

In this section, we provide a proof that  $H_3$  in (19) has global SU(2) symmetry. As in the main text, we define the total spin operators by  $S^\alpha = \sum_{j=1}^L S_j^\alpha$  ( $\alpha = x, y, z$ ), where  $S_j^\alpha$  is the spin-1 operator at site  $j$  in Eq. (16). They are the generators of the global SU(2), i.e., for any  $U \in \text{SU}(2)$  there exists  $\{\theta_\alpha\}$  such that  $U = \exp(i \sum_{\alpha \in \{x, y, z\}} \theta_\alpha S^\alpha)$ . Any  $U$  can be decomposed into  $U = 1 + X$ , where  $X$  is a polynomial in  $\{S^x, S^y, S^z\}$ . Thus, to prove that  $[H_3, U] = 0$  for all  $U \in \text{SU}(2)$ , it suffices to show  $[H_3, S^\alpha] = 0$  for all  $\alpha \in \{x, y, z\}$ .

For simplicity, we introduce the SU(3) generators  $T^a := \lambda^a/2$  satisfying  $[T^a, T^b] = i f_{abc} T^c$ , in terms of which  $H_3/8$  is written as

$$\frac{1}{8} H_3 = \sum_{j=1}^L f_{abc} T_j^a T_{j+1}^b T_{j+2}^c, \quad (\text{B1})$$

where the summation over repeated indices  $a, b$ , and  $c$  is implied. Due to the tracelessness of the SU(2) generators,  $S_j^x, S_j^y$ , and  $S_j^z$  can be written as linear combinations of the SU(3) generators. By  $\text{Tr}[T^a T^b] = \frac{1}{2} \delta_{ab}$  [131], we have  $S_j^\alpha = 2\text{Tr}_j[S_j^\alpha T_j^\mu] T_j^\mu$ . Now we calculate the commutator

$$\frac{1}{8} \left[ H_3, \sum_{k=1}^L T_k^u \right] = \left[ \sum_{j=1}^L f_{abc} T_j^a T_{j+1}^b T_{j+2}^c, \sum_{k=1}^L T_k^u \right] \quad (\text{B2})$$

$$= \sum_{j=1}^L f_{abc} ([T_j^a, T_j^u] T_{j+1}^b T_{j+2}^c + T_j^a [T_{j+1}^b, T_{j+1}^u] T_{j+2}^c + T_j^a T_{j+1}^b [T_{j+2}^c, T_{j+2}^u]) \quad (\text{B3})$$

$$= i \sum_{j=1}^L f_{abc} (f_{auv} T_j^v T_{j+1}^b T_{j+2}^c + f_{buw} T_j^a T_{j+1}^w T_{j+2}^c + f_{cuv} T_j^a T_{j+1}^b T_{j+2}^v) \quad (\text{B4})$$

$$= i \sum_{j=1}^L \underbrace{(f_{vbc} f_{vua} + f_{avc} f_{vub} + f_{abv} f_{vuc})}_{(*)} T_j^a T_{j+1}^b T_{j+2}^c. \quad (\text{B5})$$

Then it follows from the Jacobi identity that  $(*) = 0$ , which yields the desired result  $[H_3, S^\alpha] = 0$  ( $\alpha = x, y, z$ ), i.e., the global SU(2) symmetry of  $H_3$ .

**APPENDIX C: PROOF THAT  $|\Psi_{\text{VBS}}\rangle$   
IS AN INTEGRABLE BOUNDARY STATE**

In this section, we prove that the VBS state  $|\Psi_{\text{VBS}}\rangle$  in Eq. (24) is an integrable boundary state of the Sutherland model. The Hamiltonian of the model is defined as

$$H_S = - \sum_{i=1}^L (P_{i,i+1} - 1), \quad (\text{C1})$$

commuting with  $H_3$  in Sec. IV. The quantum integrability of the model can be summarized by the transfer matrix  $T(\lambda)$ ,

$$T(\lambda) = \text{Tr}_a \left( \prod_{j=1}^L R_{a,j}(\lambda) \right), \quad (\text{C2})$$

with the R matrix

$$R_{a,j}(\lambda) = \frac{1}{\lambda + i} (\lambda + iP_{a,j}) \quad (\text{C3})$$

satisfying the celebrated Yang–Baxter equation. The sub-index  $a$  stands for the three-dimensional auxiliary space, which is traced over in Eq. (C2), resulting in an operator acting only on the physical Hilbert space. From the Yang–Baxter equation, it is easy to deduce that  $T(\lambda)$  is in involution,

$$[T(\lambda), T(\mu)] = 0, \quad \forall \lambda, \mu \in \mathbb{C}. \quad (\text{C4})$$

Moreover, we have

$$H_S = -i \frac{\partial}{\partial \lambda} \log T(\lambda) \Big|_{\lambda=0}, \quad H_3 = -2i \frac{\partial^2}{\partial \lambda^2} \log T(\lambda) \Big|_{\lambda=0}. \quad (\text{C5})$$

As shown in [57], for an integrable boundary state  $|\Psi_0\rangle$  with even system size  $L$ ,

$$\begin{aligned} Q_{2k+1}|\Psi_0\rangle &= 0 \quad (k = 1, 2, \dots) \\ \Leftrightarrow T(\lambda)|\Psi_0\rangle &= \mathcal{I} T(\lambda) \mathcal{I} |\Psi_0\rangle, \end{aligned} \quad (\text{C6})$$

where the parity (spatial inversion) operator

$$\mathcal{I} = \prod_{j=1}^{L/2} P_{j,L-j+1}. \quad (\text{C7})$$

Our aim is to show that the VBS state  $|\Psi_{\text{VBS}}\rangle$  satisfies the condition (C6) with the Sutherland model transfer matrix. To begin with, for any similarity transformation with local density

$$U = \prod_{j=1}^L u_j, \quad (\text{C8})$$

the transfer matrix  $T(\lambda)$  commutes with it, i.e.,

$$\begin{aligned} UT(\lambda)U^{-1} &= \text{Tr}_a \left( \prod_{j=1}^L u_j R_{a,j}(\lambda) u_j^{-1} \right) \\ &= \text{Tr}_a \left( \prod_{j=1}^L u_a^{-1} R_{a,j}(\lambda) u_a \right) = T(\lambda), \end{aligned} \quad (\text{C9})$$

using (C3). We choose the similarity transformation to be

$$u_j = \frac{1}{\sqrt{2}} \begin{pmatrix} 1 & i & 0 \\ 0 & 0 & -\sqrt{2} \\ -1 & i & 0 \end{pmatrix}_j, \quad (\text{C10})$$

such that after acting with  $U^{-1}$  on  $|\Psi_{\text{VBS}}\rangle$ , we get [57]

$$\begin{aligned} U^{-1}|\Psi_{\text{VBS}}\rangle &= 3^{-L/2}|\Psi_0\rangle, \\ |\Psi_0\rangle &= \sum_{\{s\}} \text{Tr}[B_{s_1} B_{s_2} \cdots B_{s_L}] |s_1, s_2, \dots, s_L\rangle, \end{aligned} \quad (\text{C11})$$

where

$$B_+ = \sigma^x, \quad B_0 = \sigma^y, \quad B_- = \sigma^z. \quad (\text{C12})$$

Acting on  $|\Psi_0\rangle$  with the parity operator, we have

$$\begin{aligned} \mathcal{I}|\Psi_0\rangle &= \sum_{\{s\}} \text{Tr}[B_{s_1}^T B_{s_2}^T \cdots B_{s_L}^T] |s_1, s_2, \dots, s_L\rangle \\ &= \sum_{\{s\}} (-1)^{n_0} \text{Tr}[B_{s_1} B_{s_2} \cdots B_{s_L}] |s_1, s_2, \dots, s_L\rangle, \end{aligned} \quad (\text{C13})$$

where  $T$  denotes transpose and  $n_0$  counts the number of spin 0 in state  $|s_1, s_2, \dots, s_L\rangle$ . Since the transfer matrix  $T(\lambda)$  is a matrix product operator, we can express the state

$$\begin{aligned} T(\lambda) \text{Tr}[B_{s_1} B_{s_2} \cdots B_{s_L}] |s_1, s_2, \dots, s_L\rangle \\ = \text{Tr}[C_{s_1} C_{s_2} \cdots C_{s_L}] |s_1, s_2, \dots, s_L\rangle, \end{aligned} \quad (\text{C14})$$

where the matrices  $C_s$  ( $s = +, 0, -$ ) are 6-dimensional. In addition, one can show that there exists a similarity transformation  $V$  such that

$$C_{\pm}^T = V C_{\pm} V^{-1}, \quad C_0^T = -V C_0 V^{-1}, \quad (\text{C15})$$

i.e.,

$$\begin{aligned} \mathcal{I} \text{Tr}[C_{s_1} C_{s_2} \cdots C_{s_L}] |s_1, s_2, \dots, s_L\rangle \\ = \text{Tr}[C_{s_1}^T C_{s_2}^T \cdots C_{s_L}^T] |s_1, s_2, \dots, s_L\rangle \\ = (-1)^{n_0} \text{Tr}[C_{s_1} C_{s_2} \cdots C_{s_L}] |s_1, s_2, \dots, s_L\rangle. \end{aligned} \quad (\text{C16})$$

We are now ready to show that  $|\Psi_0\rangle$  is an integrable boundary state. Using Eqs. (C13), (C14), and (C16), we have

$$\begin{aligned} \mathcal{I} T(\lambda) \mathcal{I} |\Psi_0\rangle &= \mathcal{I} \sum_{\{s\}} (-1)^{n_0} \text{Tr}[C_{s_1} C_{s_2} \cdots C_{s_L}] |s_1, s_2, \dots, s_L\rangle \\ &= \sum_{\{s\}} (-1)^{2n_0} \text{Tr}[C_{s_1} C_{s_2} \cdots C_{s_L}] |s_1, s_2, \dots, s_L\rangle \\ &= T(\lambda) |\Psi_0\rangle. \end{aligned} \quad (\text{C17})$$

From this, we find

$$\begin{aligned} \mathcal{I} T(\lambda) \mathcal{I} |\Psi_{\text{VBS}}\rangle &= 3^{-L/2} U \mathcal{I} T(\lambda) \mathcal{I} |\Psi_0\rangle \\ &= 3^{-L/2} U T(\lambda) |\Psi_0\rangle = T(\lambda) |\Psi_{\text{VBS}}\rangle, \end{aligned} \quad (\text{C18})$$

which shows that the VBS state is an integrable boundary state of the Sutherland model.

### APPENDIX D: EIGENENERGY OF FERROMAGNETIC STATES

In this section, we compute the energy of the ferromagnetic states, which are eigenstates of the Hamiltonian  $H(t)$  in Eq. (17). The ferromagnetic states are defined as  $|F_n\rangle = (S^-)^n|F_0\rangle$ , where  $|F_0\rangle = |++\cdots+\rangle$  and  $0 \leq n \leq 2L$ . They are the same as  $|F_n\rangle_L$  with  $\sigma = 1$  in Appendix A up to a normalization factor. Because  $H_{\text{AKLT}}$  and  $H_3$  commute with  $S^-$  (see Appendix B), all ferromagnetic states  $|F_n\rangle$  have the same energy. Thus it suffices to consider the energy of  $|F_0\rangle$ .

Since  $|F_0\rangle$  is invariant under any permutation, we have  $P_{j,j+1,j+2}|F_0\rangle = P_{j,j+1,j+2}^\dagger|F_0\rangle = |F_0\rangle$ . Thus we obtain

$$H_3|F_0\rangle = \sum_{j=1}^L (P_{j,j+1,j+2} - P_{j,j+1,j+2}^\dagger)|F_0\rangle = 0, \quad (\text{D1})$$

and hence  $H_3|F_n\rangle = H_3|F_0\rangle = 0$  for all  $n$ . Moreover, since  $(S_j \cdot S_{j+1})|F_0\rangle = |F_0\rangle$  for all  $j$ , we obtain

$$H_{\text{AKLT}}|F_0\rangle = \sum_{j=1}^L \left[ 1 + \frac{1}{3} + \frac{2}{3} \right] |F_0\rangle = 2L|F_0\rangle. \quad (\text{D2})$$

Therefore, the ferromagnetic states are eigenstates of  $H(t)$  with eigenvalue  $2L$ . A similar calculation shows that the eigenenergy of the ferromagnetic states in the inhomogeneous model (30) is  $2 \sum_j c_j$ .

### APPENDIX E: PROOF OF $C_{\text{SC}}|\Psi_{\text{VBS}}\rangle = 0$

In this section, we show

$$C_{\text{SC}}|\Psi_{\text{VBS}}\rangle = 0. \quad (\text{E1})$$

First, we rewrite  $|\Psi_{\text{VBS}}\rangle$  as

$$|\Psi_{\text{VBS}}\rangle = 3^{-L/2} \text{Tr}[A_1 A_2 \cdots A_L],$$

$$A_j = \begin{pmatrix} |0\rangle_j & -\sqrt{2}|+\rangle_j \\ \sqrt{2}|-\rangle_j & -|0\rangle_j \end{pmatrix}. \quad (\text{E2})$$

Next, we introduce a convenient representation of  $C_{\text{SC}}$ ,

$$S_j \cdot (S_{j+1} \times S_{j+2}) = \frac{i}{2} \tau_{\alpha\beta\gamma} S_j^\alpha S_{j+1}^\beta S_{j+2}^\gamma, \quad (\text{E3})$$

$$\begin{aligned} B_{j,j+1,j+2} &= \frac{i}{2} \sum_{\alpha,\beta,\gamma \in \{+,-,z\}} B_{j,j+1,j+2}^{\alpha\beta\gamma} \\ &= i \begin{pmatrix} |0\rangle_+ - |-\rangle_+ + |0\rangle_- - |+\rangle_- & \sqrt{2}(|+00\rangle - |00+\rangle + |-\rangle_+ + |+\rangle_-) \\ \sqrt{2}(|00-\rangle - |-\rangle_+ - |+\rangle_-) & |+\rangle_+ + |-\rangle_+ - |0\rangle_- - |0\rangle_+ \end{pmatrix}. \end{aligned} \quad (\text{E12})$$

Then, we can decompose  $B_{j,j+1,j+2}$  into

$$B_{j,j+1,j+2} = A_j C_{j+1,j+2} - C_{j,j+1} A_{j+2}, \quad (\text{E13})$$

where

$$C_{j,j+1} = i \begin{pmatrix} |+\rangle_+ + |-\rangle_+ - |00\rangle & 0 \\ 0 & |+\rangle_+ + |-\rangle_+ - |00\rangle \end{pmatrix}. \quad (\text{E14})$$

Therefore, we have

$$C_{\text{SC}}|\Psi_{\text{VBS}}\rangle = 3^{-L/2} \sum_{j=1}^L \{ \text{Tr}[A_1 \cdots A_{j-1} A_j C_{j+1,j+2} A_{j+3} \cdots A_L] - \text{Tr}[A_1 \cdots A_{j-1} C_{j,j+1} A_{j+2} A_{j+3} \cdots A_L] \} = 0. \quad (\text{E15})$$

where  $\alpha, \beta, \gamma \in \{+, -, z\}$  and  $\tau$  is the totally antisymmetric tensor with  $\tau_{+-z} = 1$ . Then, by acting on  $|\Psi_{\text{VBS}}\rangle$  with each term, we obtain

$$\begin{aligned} \tau_{\alpha\beta\gamma} S_j^\alpha S_{j+1}^\beta S_{j+2}^\gamma |\Psi_{\text{VBS}}\rangle \\ = 3^{-L/2} \text{Tr}[A_1 \cdots A_{j-1} B_{j,j+1,j+2}^{\alpha\beta\gamma} A_{j+3} \cdots], \end{aligned} \quad (\text{E4})$$

where

$$B_{j,j+1,j+2}^{+-z} = \sqrt{2} \begin{pmatrix} |+0\rangle & -|-\rangle_+ \\ 2|00\rangle - |+\rangle_- & -\sqrt{2}|0\rangle_+ \end{pmatrix}, \quad (\text{E5})$$

$$B_{j,j+1,j+2}^{+z-} = \sqrt{2} \begin{pmatrix} 0 & -|+\rangle_+ \\ -|+\rangle_- & \sqrt{2}(|+\rangle_+ - |0\rangle_+) \end{pmatrix}, \quad (\text{E6})$$

$$B_{j,j+1,j+2}^{-z+} = \sqrt{2} \begin{pmatrix} \sqrt{2}(|0\rangle_+ - |-\rangle_+) & |-\rangle_+ \\ |-\rangle_- & 0 \end{pmatrix}, \quad (\text{E7})$$

$$B_{j,j+1,j+2}^{-+z} = \sqrt{2} \begin{pmatrix} \sqrt{2}|0\rangle_+ & |-\rangle_+ - 2|00+\rangle \\ |-\rangle_- & -\sqrt{2}|-\rangle_+ \end{pmatrix}, \quad (\text{E8})$$

$$B_{j,j+1,j+2}^{z+-} = \sqrt{2} \begin{pmatrix} -\sqrt{2}|+\rangle_+ & 2|+\rangle_+ - |+\rangle_- \\ -|-\rangle_+ & \sqrt{2}|-\rangle_+ \end{pmatrix}, \quad (\text{E9})$$

$$B_{j,j+1,j+2}^{z-+} = \sqrt{2} \begin{pmatrix} -\sqrt{2}|+\rangle_+ & |+\rangle_+ \\ |-\rangle_- - 2|-\rangle_+ & \sqrt{2}|-\rangle_+ \end{pmatrix}, \quad (\text{E10})$$

and  $B_{j,j+1,j+2}^{\alpha\beta\gamma} = 0$  for any other choice of  $(\alpha, \beta, \gamma)$ . Therefore, we obtain

$$\begin{aligned} S_j \cdot (S_{j+1} \times S_{j+2}) |\Psi_{\text{VBS}}\rangle \\ = 3^{-L/2} \text{Tr}[A_1 \cdots A_{j-1} B_{j,j+1,j+2} A_{j+3} \cdots], \end{aligned} \quad (\text{E11})$$

where

**APPENDIX F: ZERO ENERGY STATES OF  $C_{SC}$** 

In this section, we prove that  $|\bar{A}_n\rangle$ ,  $|\bar{B}_n\rangle$ , and  $|K_{0,p}\rangle$  are annihilated by  $C_{SC}$ . We also derive a lower bound on the number of zero-energy states of  $C_{SC}$ .

**1.  $C_{SC}|\bar{A}_n\rangle = 0$** 

To prove  $C_{SC}|\bar{A}_n\rangle = 0$ , we first prove the following:

*Theorem F.1.* Consider  $C_{SC}$  with an even number of sites  $L$ . Then the following relations hold:

$$C_{SC}\mathcal{O}_\pi^-|\uparrow\rangle = 0, \quad (\text{F1})$$

$$C_{SC}(\mathcal{O}_\pi^-)^2|\uparrow\rangle = 0, \quad (\text{F2})$$

$$[\mathcal{O}_\pi^-, [\mathcal{O}_\pi^-, [\mathcal{O}_\pi^-, C_{SC}]]] = 0. \quad (\text{F3})$$

*Proof.* We first prove Eq. (F1). We can write  $\mathcal{O}_\pi^-|\uparrow\rangle$  in the  $S^z$  basis as

$$\mathcal{O}_\pi^-|\uparrow\rangle = \sqrt{2} \sum_{j=1}^L (-1)^j |j\rangle, \quad (\text{F4})$$

where we have used the shorthand notation  $|j\rangle := |+\cdots+0_j+\cdots+0_j+\cdots+\rangle$ . Then we find  $C_{SC}|j\rangle = i(|j-2\rangle - |j+2\rangle)$ , which yields

$$C_{SC}\mathcal{O}_\pi^-|\uparrow\rangle = \sqrt{2}i \sum_{j=1}^L (-1)^j (|j-2\rangle - |j+2\rangle) = 0. \quad (\text{F5})$$

We can also see this as follows. First note that  $C_{SC}\mathcal{O}_\pi^-|\uparrow\rangle$  is odd under the site-centered inversion  $\mathcal{I}_s$ . We then note that it is invariant under translation by two sites  $\mathcal{T}^2$ . However, there is no single-magnon state (a linear combination of  $|j\rangle$ ) that is compatible with these constraints. Thus,  $C_{SC}\mathcal{O}_\pi^-|\uparrow\rangle$  must vanish identically.

Next, we consider Eq. (F2). By acting on  $|\uparrow\rangle$  with  $\mathcal{O}_\pi^-$  twice, we get

$$(\mathcal{O}_\pi^-)^2|\uparrow\rangle = 2 \left( 2 \sum_{1 \leq j < k \leq L} (-1)^{j+k} |j, k\rangle + \sum_{j=1}^L |\bar{j}\rangle \right), \quad (\text{F6})$$

where  $|j, k\rangle := |+\cdots+0_j+\cdots+0_k+\cdots+\rangle$  and  $|\bar{j}\rangle := |+\cdots+-_j+\cdots+\rangle$ . We can rewrite the first term as

$$\begin{aligned} & \sum_{j < k} (-1)^{j+k} |j, k\rangle \\ &= \sum_{j=1}^L \left( \sum_{r=1}^{L/2-1} (-1)^r |j, j+r\rangle + (-1)^{\frac{L}{2}} |j, j+\frac{L}{2}\rangle \right). \end{aligned} \quad (\text{F7})$$

We now examine the action of  $C_{SC}$  on  $|j, j+r\rangle$ . For  $r \geq 3$ , we get

$$\begin{aligned} C_{SC}|j, j+r\rangle &= i(|j-2, j+r\rangle - |j+2, j+r\rangle \\ &+ |j, j+r-2\rangle - |j, j+r+2\rangle) \quad (r \geq 3). \end{aligned} \quad (\text{F8})$$

Therefore, we obtain

$$C_{SC} \sum_{j=1}^L |j, j+r\rangle = 0 \quad (r \geq 3). \quad (\text{F9})$$

Next, we consider the case with  $r = 2$ . In this case, the action of  $C_{SC}$  is

$$\begin{aligned} C_{SC}|j, j+2\rangle &= i(|j-2, j+2\rangle - 2|j-1, j+2\rangle \\ &+ |j+1, j+2\rangle + |\bar{j}\rangle - |\bar{j+2}\rangle \\ &+ 2|j, j+3\rangle - |j, j+1\rangle - |j, j+4\rangle), \end{aligned} \quad (\text{F10})$$

which yields

$$C_{SC} \sum_{j=1}^L |j, j+2\rangle = 0. \quad (\text{F11})$$

Similarly, for  $|j, j+1\rangle$ , we obtain

$$\begin{aligned} C_{SC}|j, j+1\rangle &= i(|j-2, j+1\rangle - |j-1, j+1\rangle \\ &+ 2|\bar{j+1}\rangle - 2|\bar{j}\rangle + |j, j+2\rangle - |j, j+3\rangle). \end{aligned} \quad (\text{F12})$$

Thus, we have

$$\sum_{j=1}^L C_{SC}|j, j+1\rangle = 0. \quad (\text{F13})$$

We next examine  $|\bar{j}\rangle$ . Acting with  $C_{SC}$  on  $|\bar{j}\rangle$ , we obtain

$$C_{SC}|\bar{j}\rangle = i(|j-2, j\rangle - 2|j-1, j\rangle + 2|j, j+1\rangle + |j, j+2\rangle). \quad (\text{F14})$$

Thus, we have

$$\sum_{j=1}^L C_{SC}|\bar{j}\rangle = 0. \quad (\text{F15})$$

Putting this all together, we get

$$C_{SC}(\mathcal{O}_\pi^-)^2|\uparrow\rangle = 0. \quad (\text{F16})$$

Finally, we consider Eq. (F3). Since  $C_{SC}$  is a sum of terms of the form  $S_j^\alpha S_{j+1}^\beta S_{j+2}^\gamma$  ( $\{\alpha, \beta, \gamma\} = \{+, -, z\}$ ) and  $\mathcal{O}_\pi^-$  is a linear combination of  $S_k^-$ , the nested commutator  $[\mathcal{O}_\pi^-, [\mathcal{O}_\pi^-, [\mathcal{O}_\pi^-, C_{SC}]]]$  is a sum of  $S_j^- S_{j+1}^- S_{j+2}^-$ . Let  $O_j^{\alpha\beta\gamma} := [\mathcal{O}_\pi^-, [\mathcal{O}_\pi^-, [\mathcal{O}_\pi^-, S_j^\alpha S_{j+1}^\beta S_{j+2}^\gamma]]]$  for  $\{\alpha, \beta, \gamma\} = \{+, -, z\}$ , we obtain

$$\begin{aligned} O_j^{+-z} &= 3[\mathcal{O}_\pi^-, [\mathcal{O}_\pi^-, S_j^+]] S_{j+1}^- [\mathcal{O}_\pi^-, S_{j+2}^z] \\ &= 3 \cdot (-2) \cdot (-1)^{2j} S_j^- \cdot S_{j+1}^- \cdot (-1)^{j+2} S_{j+2}^- \end{aligned} \quad (\text{F17})$$

$$= -6(-1)^{j+2} S_j^- S_{j+1}^- S_{j+2}^-, \quad (\text{F18})$$

$$\begin{aligned} O_j^{-+z} &= 3S_j^- [\mathcal{O}_\pi^-, [\mathcal{O}_\pi^-, S_{j+1}^+]] [\mathcal{O}_\pi^-, S_{j+2}^z] \\ &= 3 \cdot S_j^- \cdot (-2) \cdot (-1)^{2(j+1)} S_{j+1}^- \cdot (-1)^{j+2} S_{j+2}^- \end{aligned} \quad (\text{F19})$$

$$= -6(-1)^{j+2} S_j^- S_{j+1}^- S_{j+2}^-. \quad (\text{F20})$$

Hence,  $O_j^{+-z} = O_j^{-+z}$ . Similarly, one can show that  $O_j^{-z+} = O_j^{+z-}$  and  $O_j^{z+-} = O_j^{z-+}$ . Therefore, we have

$$[\mathcal{O}_\pi^-, [\mathcal{O}_\pi^-, [\mathcal{O}_\pi^-, C_{\text{SC}}]]] = \frac{i}{2} \sum_{j=1}^L \sum_{\alpha, \beta, \gamma} \tau_{\alpha\beta\gamma} O_j^{\alpha\beta\gamma} = 0. \quad (\text{F21})$$

From Theorem F.1,  $C_{\text{SC}}|\bar{A}_n\rangle = 0$  follows immediately.

## 2. $C_{\text{SC}}|\bar{B}_n\rangle = 0$

Next we prove that  $C_{\text{SC}}|\bar{B}_n\rangle = 0$ . To this end, we first prove the following:

*Theorem F.2.* The following relations are true:

$$[\mathcal{Q}_0^-, C_{\text{SC}}]|\uparrow\rangle = 0, \quad (\text{F22})$$

$$[\mathcal{Q}_0^-, [\mathcal{Q}_0^-, C_{\text{SC}}]]|\uparrow\rangle = 0, \quad (\text{F23})$$

$$[\mathcal{Q}_0^-, [\mathcal{Q}_0^-, [\mathcal{Q}_0^-, C_{\text{SC}}]]] = 0. \quad (\text{F24})$$

*Proof.* We consider the coherent state  $|\beta\rangle$ , which can be written as

$$|\beta\rangle \propto e^{\beta \mathcal{Q}_0^-} |\uparrow\rangle = \prod_{j=1}^L (1 + \beta (S_j^-)^2) |\uparrow\rangle = \bigotimes_{j=1}^L |\psi_\beta\rangle_j, \quad (\text{F25})$$

where  $|\psi_\beta\rangle_j = |+\rangle_j + 2\beta|-\rangle_j$ . One can prove that  $|\beta\rangle$  is annihilated by  $C_{\text{SC}}$ . This can be seen as follows. First note that  $S_j^+|\psi_\beta\rangle_j = 2\sqrt{2}\beta|0\rangle_j$  and  $S_j^-|\psi_\beta\rangle_j = \sqrt{2}|0\rangle_j$ , and hence  $(S_j^+S_k^- - S_j^-S_k^+)|\psi_\beta\rangle_j \otimes |\psi_\beta\rangle_k = 0$ . Next, we note that each summand of  $C_{\text{SC}}$  can be cast in the form

$$\begin{aligned} \mathbf{S}_j \cdot (\mathbf{S}_{j+1} \times \mathbf{S}_{j+2}) &= \frac{i}{2} \{ (S_j^+ S_{j+1}^- - S_j^- S_{j+1}^+) S_{j+2}^z \\ &+ (S_{j+1}^+ S_{j+2}^- - S_{j+1}^- S_{j+2}^+) S_j^z \\ &+ (S_{j+2}^+ S_j^- - S_{j+2}^- S_j^+) S_{j+1}^z \}. \end{aligned} \quad (\text{F26})$$

From this, it is clear that each summand annihilates  $|\beta\rangle$ , and hence  $C_{\text{SC}}e^{\beta \mathcal{Q}_0^-} |\uparrow\rangle = 0$ . Acting with  $e^{-\beta \mathcal{Q}_0^-}$  from the left on both sides of this equation and expanding it by the Baker-Campbell-Hausdorff formula, we have

$$\left( C_{\text{SC}} - \beta [\mathcal{Q}_0^-, C_{\text{SC}}] + \frac{\beta^2}{2} [\mathcal{Q}_0^-, [\mathcal{Q}_0^-, C_{\text{SC}}]] + \dots \right) |\uparrow\rangle = 0, \quad (\text{F27})$$

which proves Eqs. (F22) and (F23) since  $\beta \in \mathbb{C}$  can be taken arbitrarily.

Finally, we show Eq. (F24). Let  $\mathcal{Q}_j^{\alpha\beta\gamma} = [\mathcal{Q}_0^-, [\mathcal{Q}_0^-, [\mathcal{Q}_0^-, S_j^\alpha S_{j+1}^\beta S_{j+2}^\gamma]]]$  ( $\alpha, \beta, \gamma = +, -, \text{ or } z$ ). Then, we obtain

$$\begin{aligned} \mathcal{Q}_j^{+-z} &= 3[\mathcal{Q}_0^-, [\mathcal{Q}_0^-, S_j^+]] S_{j+1}^- [\mathcal{Q}_0^-, S_{j+2}^z] \\ &= 3 \cdot (-8(S_j^-)^3) \cdot S_{j+1}^- \cdot 2(S_{j+2}^-)^2 = 0. \end{aligned} \quad (\text{F28})$$

In the same way, one can show  $\mathcal{Q}_j^{-z+} = \mathcal{Q}_j^{-z+} = \mathcal{Q}_j^{+z-} = \mathcal{Q}_j^{z+-} = \mathcal{Q}_j^{z-+} = 0$ . Therefore,

$$[\mathcal{Q}_0^-, [\mathcal{Q}_0^-, [\mathcal{Q}_0^-, C_{\text{SC}}]]] = \frac{i}{2} \sum_{j=1}^L \sum_{\alpha, \beta, \gamma} \tau_{\alpha\beta\gamma} \mathcal{Q}_j^{\alpha\beta\gamma} = 0. \quad (\text{F29})$$

From Theorem F.2,  $C_{\text{SC}}|\bar{B}_n\rangle = 0$  follows immediately.

## 3. $C_{\text{SC}}|\mathbf{K}_{0,p}\rangle = 0$

Here we prove that  $C_{\text{SC}}|\mathbf{K}_{0,p}\rangle = 0$ . From Eq. (44), each  $|\mathbf{K}_{0,p}\rangle$  can be expressed as a linear combination of  $|\Phi_n\rangle = \sum_{j=1}^L |j, j+n\rangle$ , where  $n = 0, 1, \dots, \lfloor L/2 \rfloor$  and  $|j, j\rangle = |\bar{j}\rangle$ . However, it has already been shown by Eqs. (F9), (F11), (F13), and (F15) that these states are annihilated by  $C_{\text{SC}}$ . Therefore,  $|\mathbf{K}_{0,p}\rangle$  are zero-energy states of  $C_{\text{SC}}$ .

## 4. Lower bound on the number of zero-energy states

In this subsection, we derive a lower bound on the number of zero-energy states of  $C_{\text{SC}}$ . We follow the argument in Ref. [51], where the authors obtained a lower bound on the number of zero-energy states of the PXP model. The key point is that the site-centered inversion  $\mathcal{I}_s$  anticommutes with the Hamiltonian  $C_{\text{SC}}$  in Eq. (35), i.e.,  $\mathcal{I}_s C_{\text{SC}} = -C_{\text{SC}} \mathcal{I}_s$ .

Let  $\mathcal{H}$  be the Hilbert space of a spin-1 chain of length  $L$ . This Hilbert space can be decomposed as  $\mathcal{H} = \mathcal{K}_e \oplus \mathcal{K}_o$ , where  $\mathcal{K}_e = \{|\psi\rangle \in \mathcal{H} | \mathcal{I}_s |\psi\rangle = |\psi\rangle\}$  and  $\mathcal{K}_o = \{|\psi\rangle \in \mathcal{H} | \mathcal{I}_s |\psi\rangle = -|\psi\rangle\}$ . It follows from  $\{\mathcal{I}_s, C_{\text{SC}}\} = 0$  that if  $|\psi\rangle \in \mathcal{K}_{e/o}$  then  $C_{\text{SC}}|\psi\rangle \in \mathcal{K}_{o/e}$ . Therefore,  $C_{\text{SC}}$  can be written in block-matrix form as

$$C_{\text{SC}} = \begin{pmatrix} O & D_{\text{SC}}^\dagger \\ D_{\text{SC}} & O \end{pmatrix}. \quad (\text{F30})$$

Here the operator  $D_{\text{SC}}$  can be regarded as a linear map from  $\mathcal{K}_e$  to  $\mathcal{K}_o$ . Let  $\text{Im } D_{\text{SC}}$  and  $\text{Ker } D_{\text{SC}}$  be the image and kernel of  $D_{\text{SC}}$ , respectively. It is clear that if  $|\psi\rangle \in \text{Ker } D_{\text{SC}}$ , then  $|\psi\rangle$  is annihilated by  $C_{\text{SC}}$ . Thus, the dimension of  $\text{Ker } D_{\text{SC}}$  gives a lower bound on the number of zero-energy states. We now apply the rank-nullity theorem to estimate  $\dim \text{Ker } D_{\text{SC}}$ . The theorem implies that

$$\dim \text{Im } D_{\text{SC}} + \dim \text{Ker } D_{\text{SC}} = \dim \mathcal{K}_e. \quad (\text{F31})$$

Since  $\dim \text{Im } D_{\text{SC}} \leq \dim \mathcal{K}_o$ , we have

$$\dim \text{Ker } D_{\text{SC}} \geq \dim \mathcal{K}_e - \dim \mathcal{K}_o, \quad (\text{F32})$$

which gives a lower bound on the number of zero-energy states.

Before deriving a general expression for the right-hand side of Eq. (F32), let us consider a simple example that illustrates the strategy. For  $L = 3$ , the Hilbert space  $\mathcal{H}$  is spanned by 27 states. Consider the inversion about site 2. Then  $\mathcal{K}_e$  is spanned by the states of the forms  $|s_1, s_2, s_1\rangle$  and  $|s_1, s_2, s_3\rangle + |s_3, s_2, s_1\rangle$  ( $s_1 < s_3$ ). The number of these states amounts to  $9 + 9 = 18$ . On the other hand,  $\mathcal{K}_o$  is spanned by the states of the form  $|s_1, s_2, s_3\rangle - |s_3, s_2, s_1\rangle$  ( $s_1 < s_3$ ), the number of which amounts to 9. Thus,  $\dim \mathcal{K}_e - \dim \mathcal{K}_o = 9$ .

The above example clearly illustrates that the difference between the dimensions of even and odd subspaces counts the number of product states invariant under  $\mathcal{I}_s$ . Let  $\mathcal{N}_L$  be

TABLE II. The number of zero-energy states ( $\mathcal{Z}_L$ ) and the bound ( $\mathcal{N}_L$ ) up to  $L = 11$  sites.

$L$	3	4	5	6	7	8	9	10	11
$\mathcal{Z}_L$	11	35	45	127	141	435	473	1451	1553
$\mathcal{N}_L$	9	27	27	81	81	243	243	729	729

the number of such states for the  $L$ -site system. Let  $\mathcal{Z}_L$  be the exact number of zero-energy states of  $C_{SC}$ . It is easy to see that  $\mathcal{N}_L = 3^{\lfloor \frac{L+1}{2} \rfloor}$  for  $L$  odd and  $\mathcal{N}_L = 3^{\lfloor \frac{L+2}{2} \rfloor}$  for  $L$  even. These results can be summarized as  $\mathcal{Z}_L \geq \mathcal{N}_L = 3^{\lfloor \frac{L}{2} \rfloor + 1}$ , which proves that  $\mathcal{Z}_L$  grows exponentially with the system size. Table II shows the comparison between  $\mathcal{Z}_L$  obtained by exact diagonalization and the bound  $\mathcal{N}_L$ . Clearly,  $\mathcal{Z}_L$  grows more rapidly than  $\mathcal{N}_L$ . We expect that a better lower bound can be obtained by considering other symmetries of the Hamiltonian, but leave this possibility for future work. We note in passing that a lower bound on  $\mathcal{Z}_L$  for general spin quantum number  $\sigma$  can also be derived in a similar manner; the result is  $\mathcal{Z}_L \geq (2\sigma + 1)^{\lfloor \frac{L}{2} \rfloor + 1}$ .

### APPENDIX G: TIME EVOLUTION OF A SUPERPOSITION OF $|\bar{A}_n\rangle$ and $|\bar{B}_n\rangle$

We have discussed the dynamics of the coherent states  $|\alpha\rangle$  and  $|\beta\rangle$  in Sec. VI. In this Appendix, we consider the dynamics from a more complex initial state. As we have seen, the system with the Hamiltonian  $H_2$  in Eq. (61) has two types of scar states:  $|\bar{A}_n\rangle$  and  $|\bar{B}_n\rangle$ . We will show that their superpositions exhibit more complex dynamics than those in the main text.

To be specific, let us consider the following superposition of  $|\alpha\rangle$  and  $|\beta\rangle$ :

$$|\xi\rangle = \frac{1}{Z}(u|\alpha\rangle + v|\beta\rangle), \quad (\text{G1})$$

where  $u, v \in \mathbb{C}$  are arbitrary constants and  $Z$  is the normalization constant. The fidelity between  $|\xi\rangle$  and the time evolved state  $|\xi(t)\rangle = e^{-iH_2 t}|\xi\rangle$  can be expressed as

$$\begin{aligned} \mathcal{F}(t) = |\langle \xi | \xi(t) \rangle| &= \frac{1}{Z^2} | |u|^2 \langle \alpha | \alpha(t) \rangle + u^* v \langle \alpha | \beta(t) \rangle \\ &+ uv^* \langle \beta | \alpha(t) \rangle + |v|^2 \langle \beta | \beta(t) \rangle |, \end{aligned} \quad (\text{G2})$$

where  $|\alpha(t)\rangle = e^{-iH_2 t}|\alpha\rangle$  and  $|\beta(t)\rangle = e^{-iH_2 t}|\beta\rangle$ . To get a more explicit expression for  $\mathcal{F}(t)$ , let us compute the overlaps. Along the same lines as in Eqs. (55, 63), one can calculate the first and fourth overlaps in Eq. (G2) as

$$\begin{aligned} \langle \alpha | \alpha(t) \rangle &= e^{-i\mathcal{D}(hL+\mathcal{D})t} \left( \frac{1 + |\alpha|^2 e^{iht}}{1 + |\alpha|^2} \right)^{2L}, \\ \langle \beta | \beta(t) \rangle &= e^{-i\mathcal{D}(hL+\mathcal{D})t} \left( \frac{1 + 4|\beta|^2 e^{2iht}}{1 + 4|\beta|^2} \right)^L, \end{aligned} \quad (\text{G3})$$

where  $\mathcal{D} = \sum_{j=1}^L D_j$  and we have used the fact that  $|\bar{A}_n\rangle$  and  $|\bar{B}_n\rangle$  are eigenstates of  $H_2$  with eigenvalues  $h(L-n) + \mathcal{D}$  and  $h(L-2n) + \mathcal{D}$ , respectively. Next, let us compute the second and third overlaps in Eq. (G2). To this end, we consider the overlap between  $|\bar{A}_m\rangle$  and  $|\bar{B}_n\rangle$ . Since they are eigenstates

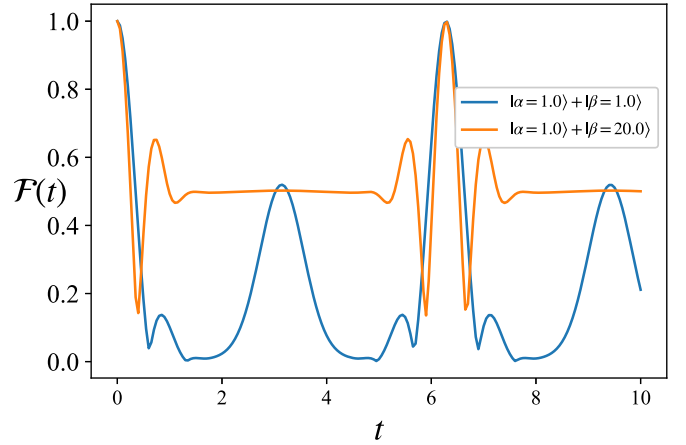


FIG. 24. The dynamics of the fidelity of the superposition of two coherent states  $|\alpha\rangle$  and  $|\beta\rangle$  driven by  $H_2$  [Eq. (61)] with  $h = 1$ ,  $L = 8$ , and  $D_j (j = 1, 2, \dots, L)$  chosen randomly from  $[-1, 1]$ . The period of the revivals is  $2\pi/h$ .

of  $S^z$  with eigenvalues  $L - m$  and  $L - 2n$ , respectively, it is easy to see that  $\langle \bar{A}_m | \bar{B}_n \rangle \propto \delta_{m,2n}$ . The overlap for  $m = 2n$  is calculated as

$$\begin{aligned} \langle \bar{A}_{2n} | \bar{B}_n \rangle &= \langle \uparrow | (O_\pi^+)^{2n} (Q_0^-)^n | \uparrow \rangle \\ &= \frac{(2n)!}{2^n} \langle \uparrow | \left( \sum_{1 \leq j_1 < \dots < j_n \leq L} (S_{j_1}^+)^2 (S_{j_2}^+)^2 \dots (S_{j_n}^+)^2 \right) | \uparrow \rangle \\ &\quad \times \left( \sum_{1 \leq l_1 < \dots < l_n \leq L} (S_{l_1}^-)^2 (S_{l_2}^-)^2 \dots (S_{l_n}^-)^2 \right) | \uparrow \rangle \\ &= 2^n \cdot (2n)! \cdot n! \cdot \binom{L}{n}, \end{aligned} \quad (\text{G4})$$

from which we obtain

$$\begin{aligned} \langle \alpha | \beta(t) \rangle &= \frac{e^{-i\mathcal{D}(hL+\mathcal{D})t} (1 + 2|\alpha^*|^2 \beta e^{2iht})^L}{(1 + |\alpha|^2)^L (1 + 4|\beta|^2)^{\frac{L}{2}}}, \\ \langle \beta | \alpha(t) \rangle &= \frac{e^{-i\mathcal{D}(hL+\mathcal{D})t} (1 + 2\alpha^2 \beta^* e^{2iht})^L}{(1 + |\alpha|^2)^L (1 + 4|\beta|^2)^{\frac{L}{2}}}. \end{aligned} \quad (\text{G5})$$

Plugging Eqs. (G3) and (G5) into Eq. (G2) yields

$$\begin{aligned} \mathcal{F}(t) &= \frac{1}{Z^2} \left| |u|^2 \left( \frac{1 + |\alpha|^2 e^{iht}}{1 + |\alpha|^2} \right)^{2L} + |v|^2 \left( \frac{1 + 4|\beta|^2 e^{2iht}}{1 + 4|\beta|^2} \right)^L \right. \\ &\quad \left. + u^* v \frac{(1 + 2|\alpha^*|^2 \beta e^{2iht})^L}{(1 + |\alpha|^2)^L (1 + 4|\beta|^2)^{\frac{L}{2}}} \right. \\ &\quad \left. + uv^* \frac{(1 + 2\alpha^2 \beta^* e^{2iht})^L}{(1 + |\alpha|^2)^L (1 + 4|\beta|^2)^{\frac{L}{2}}} \right|, \end{aligned} \quad (\text{G6})$$

with

$$Z^2 = \left| |u|^2 + |v|^2 + \frac{2\Re[u^* v (1 + 2|\alpha^*|^2 \beta)]}{(1 + |\alpha|^2)^L (1 + 4|\beta|^2)^{\frac{L}{2}}} \right|. \quad (\text{G7})$$

Figure 24 shows  $\mathcal{F}(t)$  for two different choices of  $(\alpha, \beta)$ . We can see that the fidelity shows revivals with period  $2\pi/h$ , which is the smallest common period of the two fidelity

oscillations shown in Figs. 18 and 21. Clearly, the trend of the curves is more complicated than the previous ones, with

small peaks originating from the interference terms  $\langle\alpha|\beta(t)\rangle$  and  $\langle\beta|\alpha(t)\rangle$ .

- [1] S. Trotzky, Y.-A. Chen, A. Flesch, I. P. McCulloch, U. Schollwöck, J. Eisert, and I. Bloch, Probing the relaxation towards equilibrium in an isolated strongly correlated one-dimensional Bose gas, *Nat. Phys.* **8**, 325 (2012).
- [2] C. Neill, P. Roushan, M. Fang, Y. Chen, M. Kolodrubetz, Z. Chen, A. Megrant, R. Barends, B. Campbell, B. Chiaro *et al.*, Ergodic dynamics and thermalization in an isolated quantum system, *Nat. Phys.* **12**, 1037 (2016).
- [3] J. Smith, A. Lee, P. Richerme, B. Neyenhuis, P. W. Hess, P. Hauke, M. Heyl, D. A. Huse, and C. Monroe, Many-body localization in a quantum simulator with programmable random disorder, *Nat. Phys.* **12**, 907 (2016).
- [4] H. Bernien, S. Schwartz, A. Keesling, H. Levine, A. Omran, H. Pichler, S. Choi, A. S. Zibrov, M. Endres, M. Greiner *et al.*, Probing many-body dynamics on a 51-atom quantum simulator, *Nature (London)* **551**, 579 (2017).
- [5] J. von Neumann, Proof of the ergodic theorem and the H-theorem in quantum mechanics, *Eur. Phys. J. H* **35**, 201 (2010); Beweis des Ergodensatzes und des H-Theorems in der neuen Mechanik, *Z. Phys.* **57**, 30 (1929).
- [6] S. Goldstein, J. L. Lebowitz, R. Tumulka, and N. Zanghi, Long-time behavior of macroscopic quantum systems: Commentary accompanying the English translation of John von Neumann's 1929 article on the quantum ergodic theorem, *Eur. Phys. J. H* **35**, 173 (2010).
- [7] M. Rigol and M. Srednicki, Alternatives to eigenstate thermalization, *Phys. Rev. Lett.* **108**, 110601 (2012).
- [8] H. Tasaki, From quantum dynamics to the canonical distribution: General picture and a rigorous example, *Phys. Rev. Lett.* **80**, 1373 (1998).
- [9] J. M. Deutsch, Quantum statistical mechanics in a closed system, *Phys. Rev. A* **43**, 2046 (1991).
- [10] M. Srednicki, Chaos and quantum thermalization, *Phys. Rev. E* **50**, 888 (1994).
- [11] M. Horoi, V. Zelevinsky, and B. A. Brown, Chaos vs thermalization in the nuclear shell model, *Phys. Rev. Lett.* **74**, 5194 (1995).
- [12] V. Zelevinsky, B. A. Brown, N. Frazier, and M. Horoi, The nuclear shell model as a testing ground for many-body quantum chaos, *Phys. Rep.* **276**, 85 (1996).
- [13] L. C. Venuti and L. Liu, Ergodicity, eigenstate thermalization, and the foundations of statistical mechanics in quantum and classical systems, [arXiv:1904.02336](https://arxiv.org/abs/1904.02336).
- [14] J. M. Deutsch, Eigenstate thermalization hypothesis, *Rep. Prog. Phys.* **81**, 082001 (2018).
- [15] In contrast, the weak ETH claims that almost all energy eigenstates are thermal, which allows a small number of exceptional eigenstates called nonthermal states. Actually, the weak ETH has been proved in some cases [132,133].
- [16] M. Rigol, V. Dunjko, and M. Olshanii, Thermalization and its mechanism for generic isolated quantum systems, *Nature (London)* **452**, 854 (2008).
- [17] A. Polkovnikov, K. Sengupta, A. Silva, and M. Vengalattore, Colloquium: Nonequilibrium dynamics of closed interacting quantum systems, *Rev. Mod. Phys.* **83**, 863 (2011).
- [18] R. Nandkishore and D. A. Huse, Many-body localization and thermalization in quantum statistical mechanics, *Annu. Rev. Condens. Matter Phys.* **6**, 15 (2015).
- [19] Unfortunately, it was reported that there is no general theorem, algorithm, or systematic procedure to determine whether any given quantum many-body system thermalizes or not [134].
- [20] M. Serbyn, D. A. Abanin, and Z. Papić, Quantum many-body scars and weak breaking of ergodicity, *Nat. Phys.* **17**, 675 (2021).
- [21] S. Moudgalya, N. Regnault, and B. A. Bernevig, Quantum many-body scars and hilbert space fragmentation: A review of exact results, *Rep. Prog. Phys.* **85**, 086501 (2022).
- [22] A. Chandran, T. Iadecola, V. Khemani, and R. Moessner, Quantum many-body scars: A quasiparticle perspective, *Annu. Rev. Condens. Matter Phys.* **14**, 443 (2023).
- [23] G.-X. Su, H. Sun, A. Hudomal, J.-Y. Desaulles, Z.-Y. Zhou, B. Yang, J. C. Halimeh, Z.-S. Yuan, Z. Papić, and J.-W. Pan, Observation of many-body scarring in a Bose-Hubbard quantum simulator, *Phys. Rev. Res.* **5**, 023010 (2023).
- [24] P. Zhang, H. Dong, Y. Gao, L. Zhao, J. Hao, J.-Y. Desaulles, Q. Guo, J. Chen, J. Deng, B. Liu *et al.*, Many-body Hilbert space scarring on a superconducting processor, *Nat. Phys.* **19**, 120 (2023).
- [25] A. Hudomal, I. Vasić, N. Regnault, and Z. Papić, Quantum scars of bosons with correlated hopping, *Commun. Phys.* **3**, 99 (2020).
- [26] H. Zhao, J. Vovrosh, F. Mintert, and J. Knolle, Quantum many-body scars in optical lattices, *Phys. Rev. Lett.* **124**, 160604 (2020).
- [27] J.-Y. Desaulles, A. Hudomal, C. J. Turner, and Z. Papić, Proposal for realizing quantum scars in the tilted 1D Fermi-Hubbard model, *Phys. Rev. Lett.* **126**, 210601 (2021).
- [28] M. Kunimi, T. Tomita, H. Katsura, and Y. Kato, Proposal for realizing quantum spin models with Dzyaloshinskii-Moriya interaction using Rydberg atoms, [arXiv:2306.05591](https://arxiv.org/abs/2306.05591).
- [29] C. J. Turner, A. A. Michailidis, D. A. Abanin, M. Serbyn, and Z. Papić, Weak ergodicity breaking from quantum many-body scars, *Nat. Phys.* **14**, 745 (2018).
- [30] S. Choi, C. J. Turner, H. Pichler, W. W. Ho, A. A. Michailidis, Z. Papić, M. Serbyn, M. D. Lukin, and D. A. Abanin, Emergent SU(2) dynamics and perfect quantum many-body scars, *Phys. Rev. Lett.* **122**, 220603 (2019).
- [31] C.-J. Lin and O. I. Motrunich, Exact quantum many-body scar states in the Rydberg-blockaded atom chain, *Phys. Rev. Lett.* **122**, 173401 (2019).
- [32] N. Shiraishi, Connection between quantum-many-body scars and the Affleck-Kennedy-Lieb-Tasaki model from the viewpoint of embedded Hamiltonians, *J. Stat. Mech. Theory Exp.* (2019) 083103.
- [33] C.-J. Lin, V. Calvera, and T. H. Hsieh, Quantum many-body scar states in two-dimensional Rydberg atom arrays, *Phys. Rev. B* **101**, 220304(R) (2020).
- [34] S. Moudgalya, N. Regnault, and B. A. Bernevig, Entanglement of exact excited states of Affleck-Kennedy-Lieb-Tasaki models: Exact results, many-body scars, and violation of the strong

- eigenstate thermalization hypothesis, *Phys. Rev. B* **98**, 235156 (2018).
- [35] D. K. Mark, C.-J. Lin, and O. I. Motrunich, Unified structure for exact towers of scar states in the Affleck-Kennedy-Lieb-Tasaki and other models, *Phys. Rev. B* **101**, 195131 (2020).
- [36] N. O’Dea, F. Burnell, A. Chandran, and V. Khemani, From tunnels to towers: Quantum scars from Lie algebras and  $q$ -deformed Lie algebras, *Phys. Rev. Res.* **2**, 043305 (2020).
- [37] M. Schecter and T. Iadecola, Weak ergodicity breaking and quantum many-body scars in spin-1  $XY$  magnets, *Phys. Rev. Lett.* **123**, 147201 (2019).
- [38] T. Iadecola and M. Schecter, Quantum many-body scar states with emergent kinetic constraints and finite-entanglement revivals, *Phys. Rev. B* **101**, 024306 (2020).
- [39] S. Chattopadhyay, H. Pichler, M. D. Lukin, and W. W. Ho, Quantum many-body scars from virtual entangled pairs, *Phys. Rev. B* **101**, 174308 (2020).
- [40] S. Moudgalya, E. O’Brien, B. A. Bernevig, P. Fendley, and N. Regnault, Large classes of quantum scarred Hamiltonians from matrix product states, *Phys. Rev. B* **102**, 085120 (2020).
- [41] N. Shibata, N. Yoshioka, and H. Katsura, Onsager’s scars in disordered spin chains, *Phys. Rev. Lett.* **124**, 180604 (2020).
- [42] N. Shiraishi and T. Mori, Systematic construction of counterexamples to the eigenstate thermalization hypothesis, *Phys. Rev. Lett.* **119**, 030601 (2017).
- [43] P. A. McClarty, M. Haque, A. Sen, and J. Richter, Disorder-free localization and many-body quantum scars from magnetic frustration, *Phys. Rev. B* **102**, 224303 (2020).
- [44] K. Pakrouski, P. N. Pallegar, F. K. Popov, and I. R. Klebanov, Many-body scars as a group invariant sector of Hilbert space, *Phys. Rev. Lett.* **125**, 230602 (2020).
- [45] K. Pakrouski, P. N. Pallegar, F. K. Popov, and I. R. Klebanov, Group theoretic approach to many-body scar states in fermionic lattice models, *Phys. Rev. Res.* **3**, 043156 (2021).
- [46] J. Ren, C. Liang, and C. Fang, Quasisymmetry groups and many-body scar dynamics, *Phys. Rev. Lett.* **126**, 120604 (2021).
- [47] L.-H. Tang, N. O’Dea, and A. Chandran, Multimagnon quantum many-body scars from tensor operators, *Phys. Rev. Res.* **4**, 043006 (2022).
- [48] J. Wildeboer, C. M. Langlett, Z.-C. Yang, A. V. Gorshkov, T. Iadecola, and S. Xu, Quantum many-body scars from Einstein-Podolsky-Rosen states in bilayer systems, *Phys. Rev. B* **106**, 205142 (2022).
- [49] J. Ren, C. Liang, and C. Fang, Deformed symmetry structures and quantum many-body scar subspaces, *Phys. Rev. Res.* **4**, 013155 (2022).
- [50] K. Omiya and M. Müller, Fractionalization paves the way to local projector embeddings of quantum many-body scars, *Phys. Rev. B* **108**, 054412 (2023).
- [51] C. J. Turner, A. A. Michailidis, D. A. Abanin, M. Serbyn, and Z. Papić, Quantum scarred eigenstates in a Rydberg atom chain: Entanglement, breakdown of thermalization, and stability to perturbations, *Phys. Rev. B* **98**, 155134 (2018).
- [52] C.-J. Lin, A. Chandran, and O. I. Motrunich, Slow thermalization of exact quantum many-body scar states under perturbations, *Phys. Rev. Res.* **2**, 033044 (2020).
- [53] L. Gotta, S. Moudgalya, and L. Mazza, Asymptotic quantum many-body scars, [arXiv:2303.05407](https://arxiv.org/abs/2303.05407).
- [54] S. Moudgalya and O. I. Motrunich, Exhaustive characterization of quantum many-body scars using commutant algebras, [arXiv:2209.03377](https://arxiv.org/abs/2209.03377).
- [55] S. Moudgalya and O. I. Motrunich, Hilbert space fragmentation and commutant algebras, *Phys. Rev. X* **12**, 011050 (2022).
- [56] M. de Leeuw, C. Kristjansen, and K. Zarembo, One-point functions in defect CFT and integrability, *J. High Energy Phys.* **08** (2015) 098.
- [57] L. Piroli, B. Pozsgay, and E. Vernier, What is an integrable quench, *Nucl. Phys.* **925**, 362 (2017).
- [58] M. De Leeuw, C. Kristjansen, and G. Linardopoulos, Scalar one-point functions and matrix product states of AdS/dCFT, *Phys. Lett. B* **781**, 238 (2018).
- [59] B. Pozsgay, Overlaps with arbitrary two-site states in the XXZ spin chain, *J. Stat. Mech.: Theory Exp.* (2018) 053103.
- [60] L. Piroli, E. Vernier, P. Calabrese, and B. Pozsgay, Integrable quenches in nested spin chains I: The exact steady states, *J. Stat. Mech.* (2019) 063103.
- [61] B. Pozsgay, L. Piroli, and E. Vernier, Integrable matrix product states from boundary integrability, *SciPost Phys.* **6**, 062 (2019).
- [62] S. Moudgalya, N. Regnault, and B. A. Bernevig,  $\eta$ -pairing in Hubbard models: From spectrum generating algebras to quantum many-body scars, *Phys. Rev. B* **102**, 085140 (2020).
- [63] B. Buča, J. Tindall, and D. Jaksch, Non-stationary coherent quantum many-body dynamics through dissipation, *Nat. Commun.* **10**, 1730 (2019).
- [64] E. Sklyanin, Quantum inverse scattering method. Selected topics, [arXiv:hep-th/9211111](https://arxiv.org/abs/hep-th/9211111).
- [65] M. Grabowski and P. Mathieu, Structure of the conservation laws in quantum integrable spin chains with short range interactions, *Ann. Phys.* **243**, 299 (1995).
- [66] M. De Leeuw, A. Pribytok, and P. Ryan, Classifying integrable spin-1/2 chains with nearest neighbour interactions, *J. Phys. A: Math. Theor.* **52**, 505201 (2019).
- [67] The boost operator also works for non-difference-form R matrices, see Ref. [66].
- [68] M. V. Berry and M. Tabor, Level clustering in the regular spectrum, *Proc. R. Soc. London A* **356**, 375 (1977).
- [69] M. V. Berry, Quantizing a classically ergodic system: Sinai’s billiard and the KKR method, *Ann. Phys.* **131**, 163 (1981).
- [70] O. Bohigas, M. J. Giannoni, and C. Schmit, Characterization of chaotic quantum spectra and universality of level fluctuation laws, *Phys. Rev. Lett.* **52**, 1 (1984).
- [71] D. Szász-Schagrin, B. Pozsgay, and G. Takács, Weak integrability breaking and level spacing distribution, *SciPost Phys.* **11**, 037 (2021).
- [72] M. Gaudin, Sur la loi limite de l’espacement des valeurs propres d’une matrice ale’atoire, *Nucl. Phys.* **25**, 447 (1961).
- [73] V. Oganesyan and D. A. Huse, Localization of interacting fermions at high temperature, *Phys. Rev. B* **75**, 155111 (2007).
- [74] Y. Y. Atas, E. Bogomolny, O. Giraud, and G. Roux, Distribution of the ratio of consecutive level spacings in random matrix ensembles, *Phys. Rev. Lett.* **110**, 084101 (2013).
- [75] T. Mori, T. N. Ikeda, E. Kaminishi, and M. Ueda, Thermalization and prethermalization in isolated quantum systems: A theoretical overview, *J. Phys. B: At. Mol. Opt. Phys.* **51**, 112001 (2018).

- [76] C. K. Majumdar and D. K. Ghosh, On next-nearest-neighbor interaction in linear chain. I, *J. Math. Phys.* **10**, 1388 (1969).
- [77] C. K. Majumdar and D. K. Ghosh, On next-nearest-neighbor interaction in linear chain. II, *J. Math. Phys.* **10**, 1399 (1969).
- [78] W. J. Caspers, K. M. Emmett, and W. Magnus, The majumdar-ghosh chain. twofold ground state and elementary excitations, *J. Phys. A: Math. Gen.* **17**, 2687 (1984).
- [79] X. G. Wen, F. Wilczek, and A. Zee, Chiral spin states and superconductivity, *Phys. Rev. B* **39**, 11413 (1989).
- [80] H. Frahm and C. Rödenbeck, Properties of the chiral spin liquid state in generalized spin ladders, *J. Phys. A: Math. Gen.* **30**, 4467 (1997).
- [81] D. Sen and R. Chitra, Large- $U$  limit of a Hubbard model in a magnetic field: Chiral spin interactions and paramagnetism, *Phys. Rev. B* **51**, 1922 (1995).
- [82] K. Kim, F. Yang, K. Mølmer, and J. Ahn, Realization of an extremely anisotropic Heisenberg magnet in Rydberg atom arrays, [arXiv:2307.04342](https://arxiv.org/abs/2307.04342).
- [83] The group  $\{1, \mathcal{F}\}$  is a discrete subgroup of  $SU(2)$ , where  $\mathcal{F}$  corresponds to a  $\pi$  rotation around the  $x$  axis.
- [84] M. S. Ramkarthik, V. R. Chandra, and A. Lakshminarayan, Entanglement signatures for the dimerization transition in the Majumdar-Ghosh model, *Phys. Rev. A* **87**, 012302 (2013).
- [85] V. Popkov and M. Salerno, Logarithmic divergence of the block entanglement entropy for the ferromagnetic Heisenberg model, *Phys. Rev. A* **71**, 012301 (2005).
- [86] M. P. Grabowski and P. Mathieu, Quantum integrals of motion for the Heisenberg spin chain, *Mod. Phys. Lett. A* **09**, 2197 (1994).
- [87] I. Affleck, T. Kennedy, E. H. Lieb, and H. Tasaki, Rigorous results on valence-bond ground states in antiferromagnets, *Phys. Rev. Lett.* **59**, 799 (1987).
- [88] I. Affleck, T. Kennedy, E. H. Lieb, and H. Tasaki, Valence bond ground states in isotropic quantum antiferromagnets, *Commun. Math. Phys.* **115**, 477 (1988).
- [89] H. Tasaki, *Physics and Mathematics of Quantum Many-Body Systems* (Springer, New York, 2020).
- [90] B. Sutherland, Model for a multicomponent quantum system, *Phys. Rev. B* **12**, 3795 (1975).
- [91] C. K. Lai, Lattice gas with nearest-neighbor interaction in one dimension with arbitrary statistics, *J. Math. Phys.* **15**, 1675 (1974).
- [92] G. V. Uimin, One-dimensional problem for  $S = 1$  with modified antiferromagnetic Hamiltonian, *Zh. Eksp. Teor. Fiz. Pis. Red.* **12**, 332 (1970) [*JETP Lett.* **12**, 225 (1970)].
- [93] M. P. Grabowski and P. Mathieu, Integrability test for spin chains, *J. Phys. A: Math. Gen.* **28**, 4777 (1995).
- [94] Y.-T. Oh, H. Katsura, H.-Y. Lee, and J. H. Han, Proposal of a spin-one chain model with competing dimer and trimer interactions, *Phys. Rev. B* **96**, 165126 (2017).
- [95] J.-Y. Chen, S. Capponi, A. Wietek, M. Mambrini, N. Schuch, and D. Poilblanc,  $SU(3)_1$  chiral spin liquid on the square lattice: A view from symmetric projected entangled pair states, *Phys. Rev. Lett.* **125**, 017201 (2020).
- [96] S. Schierenberg, F. Bruckmann, and T. Wettig, Wigner surmise for mixed symmetry classes in random matrix theory, *Phys. Rev. E* **85**, 061130 (2012).
- [97] D. Kundu, S. Kumar, and S. Sen Gupta, Signatures of spectral crossovers in the short-and long-range spectral correlations of a disordered spin-chain with Kramers degeneracy, *Phys. Rev. B* **107**, 094205 (2023).
- [98] T. Hirano and Y. Hatsugai, Entanglement entropy of one-dimensional gapped spin chains, *J. Phys. Soc. Jpn.* **76**, 074603 (2007).
- [99] H. Katsura, T. Hirano, and Y. Hatsugai, Exact analysis of entanglement in gapped quantum spin chains, *Phys. Rev. B* **76**, 012401 (2007).
- [100] C. Lange, A. Klümper, and J. Zittartz, Exact groundstates for antiferromagnetic spin-one chains with nearest and next-nearest neighbour interactions, *Z. Phys. B* **96**, 267 (1994).
- [101] H. Nakano and M. Takahashi, Long-ranged interacting  $S = 1$  spin chain with the exact valence-bond-solid state, *Phys. Rev. B* **54**, 9000 (1996).
- [102] D. Scalapino, S.-C. Zhang, and W. Hanke,  $SO(5)$  symmetric ladder, *Phys. Rev. B* **58**, 443 (1998).
- [103] H. Frahm and M. Stahlsmeier, Electronic ladders with  $SO(5)$  symmetry: Phase diagrams and correlations at half filling, *Phys. Rev. B* **63**, 125109 (2001).
- [104] H.-H. Tu, G.-M. Zhang, and T. Xiang, Class of exactly solvable  $SO(n)$  symmetric spin chains with matrix product ground states, *Phys. Rev. B* **78**, 094404 (2008).
- [105] K. Lee, R. Melendrez, A. Pal, and H. J. Changlani, Exact three-colored quantum scars from geometric frustration, *Phys. Rev. B* **101**, 241111(R) (2020).
- [106] K. Lee, A. Pal, and H. J. Changlani, Frustration-induced emergent Hilbert space fragmentation, *Phys. Rev. B* **103**, 235133 (2021).
- [107] Á. M. Alhambra, A. Anshu, and H. Wilming, Revivals imply quantum many-body scars, *Phys. Rev. B* **101**, 205107 (2020).
- [108] Y.-Y. Shi, L.-M. Duan, and G. Vidal, Classical simulation of quantum many-body systems with a tree tensor network, *Phys. Rev. A* **74**, 022320 (2006).
- [109] H. Katsura, N. Kawashima, A. N. Kirillov, V. E. Korepin, and S. Tanaka, Entanglement in valence-bond-solid states on symmetric graphs, *J. Phys. A: Math. Theor.* **43**, 255303 (2010).
- [110] D. N. Page, Average entropy of a subsystem, *Phys. Rev. Lett.* **71**, 1291 (1993).
- [111] S. Ghoshal and A. Zamolodchikov, Boundary S matrix and boundary state in two-dimensional integrable quantum field theory, *Int. J. Mod. Phys. A* **09**, 3841 (1994).
- [112] F. Schindler, N. Regnault, and B. A. Bernevig, Exact quantum scars in the chiral nonlinear Luttinger liquid, *Phys. Rev. B* **105**, 035146 (2022).
- [113] I. Martin and K. A. Matveev, Scar states in a system of interacting chiral fermions, *Phys. Rev. B* **105**, 045119 (2022).
- [114] D. Liska, V. Gritsev, W. Vleeshouwers, and J. Minář, Holographic quantum scars, *SciPost Phys.* **15**, 106 (2023).
- [115] J. Cotler and A. Y. Wei, Quantum scars in quantum field theory, *Phys. Rev. D* **107**, 125005 (2023).
- [116] F. Iemini, A. Russomanno, J. Keeling, M. Schirò, M. Dalmonte, and R. Fazio, Boundary time crystals, *Phys. Rev. Lett.* **121**, 035301 (2018).
- [117] S. Dutta and N. R. Cooper, Out-of-equilibrium steady states of a locally driven lossy qubit array, *Phys. Rev. Res.* **3**, L012016 (2021).
- [118] J. Tindall, F. Schlawin, M. A. Sentef, and D. Jaksch, Analytical solution for the steady states of the driven Hubbard model, *Phys. Rev. B* **103**, 035146 (2021).

- [119] B. Buča, C. Booker, and D. Jaksch, Algebraic theory of quantum synchronization and limit cycles under dissipation, *SciPost Phys.* **12**, 097 (2022).
- [120] A. A. Ziolkowska and F. Essler, Yang-Baxter integrable Lindblad equations, *SciPost Phys.* **8**, 044 (2020).
- [121] M. de Leeuw, C. Paletta, and B. Pozsgay, Constructing integrable Lindblad superoperators, *Phys. Rev. Lett.* **126**, 240403 (2021).
- [122] M. de Leeuw, C. Paletta, B. Pozsgay, and E. Vernier, Hidden quasi-local charges and Gibbs ensemble in a Lindblad system, [arXiv:2305.01922](https://arxiv.org/abs/2305.01922).
- [123] V. Gritsev and A. Polkovnikov, Integrable Floquet dynamics, *SciPost Phys.* **2**, 021 (2017).
- [124] M. Vanicat, L. Zadnik, and T. Prosen, Integrable Trotterization: Local conservation laws and boundary driving, *Phys. Rev. Lett.* **121**, 030606 (2018).
- [125] A. I. Lotkov, V. Gritsev, A. K. Fedorov, and D. V. Kurlov, Floquet integrability and long-range entanglement generation in the one-dimensional quantum Potts model, *Phys. Rev. B* **105**, 144306 (2022).
- [126] P. Weinberg and M. Bukov, QuSpin: A python package for dynamics and exact diagonalisation of quantum many body systems part I: Spin chains, *SciPost Phys.* **2**, 003 (2017).
- [127] P. Weinberg and M. Bukov, QuSpin: A python package for dynamics and exact diagonalisation of quantum many body systems. part II: Bosons, fermions and higher spins, *SciPost Phys.* **7**, 020 (2019).
- [128] C. Eliot, Probability distributions, in *Probability, Statistics, and Queuing Theory with Computer Science Applications (Second Edition)*, Computer Science and Scientific Computing, edited by A. O. Allen (Academic Press, San Diego, 1990), Chap. 3, pp. 109–198.
- [129] J. V. Uspensky, *Introduction to Mathematical Probability* (McGraw-Hill, New York, 1937).
- [130] F. Diener and M. Diener, Higher-order terms for the de Moivre-Laplace theorem, *Contemp. Math.* **373**, 191 (2005).
- [131] H. Georgi, *Lie Algebras in Particle Physics: From Isospin to Unified Theories* (Taylor & Francis, London, 2000).
- [132] G. Biroli, C. Kollath, and A. M. Läuchli, Effect of rare fluctuations on the thermalization of isolated quantum systems, *Phys. Rev. Lett.* **105**, 250401 (2010).
- [133] E. Iyoda, K. Kaneko, and T. Sagawa, Fluctuation theorem for many-body pure quantum states, *Phys. Rev. Lett.* **119**, 100601 (2017).
- [134] N. Shiraishi and K. Matsumoto, Undecidability in quantum thermalization, *Nat. Commun.* **12**, 5084 (2021).